



RADIO DETECTION PROSPECTS FOR A BULGE POPULATION OF MILLISECOND PULSARS AS SUGGESTED BY FERMI-LAT OBSERVATIONS OF THE INNER GALAXY

F. CALORE¹, M. DI MAURO², F. DONATO^{3,4}, J. W. T. HESSELS^{5,6}, AND C. WENIGER¹

¹ GRAPPA Institute, University of Amsterdam, Science Park 904, 1090 GL Amsterdam, Netherlands; f.calore@uva.nl, c.weniger@uva.nl

² Department of Physics and SLAC National Accelerator Laboratory, Stanford University, Stanford, CA 94305, USA

³ Physics Department, Torino University, via Giuria 1, I-10125 Torino, Italy

⁴ Istituto Nazionale di Fisica Nucleare, Sezione di Torino, via Giuria 1, I-10125 Torino, Italy

⁵ ASTRON, the Netherlands Institute for Radio Astronomy, Postbus 2, 7990 AA, Dwingeloo, The Netherlands

⁶ Anton Pannekoek Institute for Astronomy, University of Amsterdam, Science Park 904, 1098 XH Amsterdam, The Netherlands

Received 2016 January 25; revised 2016 May 17; accepted 2016 May 18; published 2016 August 18

ABSTRACT

The dense stellar environment of the Galactic center has been proposed to host a large population of as-yet undetected millisecond pulsars (MSPs). Recently, this hypothesis has found support in an analysis of gamma-rays detected using the Large Area Telescope onboard the *Fermi* satellite, which revealed an excess of diffuse GeV photons in the inner 15 deg about the Galactic center. The excess can be interpreted as the collective emission of thousands of MSPs in the Galactic bulge, with a spherical distribution strongly peaked toward the Galactic center. In order to fully establish the MSP interpretation, it is essential to find corroborating evidence in multi-wavelength searches, most notably through the detection of radio pulsations from individual bulge MSPs. Based on globular cluster observations and gamma-ray emission from the inner Galaxy, we investigate the prospects for detecting MSPs in the Galactic bulge. While previous pulsar surveys failed to identify this population, we demonstrate that upcoming large-area surveys of this region should lead to the detection of dozens of bulge MSPs. Additionally, we show that deep targeted searches of unassociated *Fermi* sources should be able to detect the first few MSPs in the bulge. The prospects for these deep searches are enhanced by a tentative gamma-ray/radio correlation that we infer from high-latitude gamma-ray MSPs. Such detections would constitute the first clear discoveries of field MSPs in the Galactic bulge, with far-reaching implications for gamma-ray observations, the formation history of the central Milky Way, and strategy optimization for future deep radio pulsar surveys.

Key words: astroparticle physics – gamma-rays: diffuse background – pulsars: general – radio continuum: general – radio continuum: stars

1. INTRODUCTION

Millisecond pulsars (MSPs) are rapidly spinning neutron stars that produce observable pulsations (mostly in radio, but often also in gamma-rays, and occasionally in X-rays), have short spin periods, and low surface magnetic fields (compared to other pulsars) that are loosely in the range $P \leq 30$ ms and $B \leq 10^9$ G. MSPs are believed to originate from pulsars in binary systems in which the companion star transfers material to the pulsar, reducing its magnetic field and increasing its angular momentum. During the accretion phase, and for low-mass companions, the system can often be seen as a low-mass X-ray binary. Afterwards, an MSP (for that reason also called *recycled* pulsar) is left behind and can emit observable pulsations for about 10^{10} years (Bhattacharya & van den Heuvel 1991).

MSPs have a multi-wavelength emission spectrum, including both pulsed and un-pulsed types of emission, from radio frequencies up to TeV gamma-rays. MSPs emit soft X-rays through the polar caps ($kT \leq 1$ keV, Zhang & Cheng 2003). They can also shine in GeV gamma-rays through curvature radiation as predicted by outer gap models (Zhang & Cheng 2003). We refer to the recent review by Grenier & Harding (2015) for further details and references. Strong pulsar winds, accelerating relativistic electrons interacting with the surrounding medium, might be responsible for non-pulsed X-ray emission through synchrotron radiation (Chevalier 2000; Cheng et al. 2004) and for TeV photons through inverse Compton scattering (Aharonian et al. 1997). The detailed

timing of the multi-wavelength emission provides useful information to study emission models (e.g., Kalapotharakos et al. 2014).

About 370 MSPs are currently known at radio frequencies: 237 of them are field MSPs in the Galactic disk,⁷ and 133 (with $P \leq 30$ ms) are associated with 28 different globular clusters.⁸ Historically, the first ~ 35 field MSPs were found in the 1980s and 1990s in large area radio surveys, mainly based on the Parkes southern sky survey and the Arecibo survey at 430 MHz. Subsequently, various large area surveys using again the Parkes telescope, Arecibo, and since 2002 also the Green Bank Telescope (GBT), lead to the discovery of around 200 MSPs (for a recent review see Stovall et al. 2013). Additionally, ~ 70 MSPs were discovered in radio follow-ups of *Fermi* unassociated sources (Ray et al. 2012), and at least one MSP was first detected by observing gamma-ray pulsations (Abdo et al. 2013). All MSPs in globular clusters were instead found in deep targeted searches.

The presence of gamma-ray and radio MSPs in the Galactic disk and in globular clusters is now well established (Abdo et al. 2010, 2013). Additionally, it has been long proposed that the Galactic center might harbor an MSP population with a much larger number density than the Galactic disk. One traditional argument (Macquart & Kanekar 2015) supporting this hypothesis is that the high stellar density at the Galactic center is substantially different from the disk. In such a highly

⁷ <http://astro.phys.wvu.edu/GalacticMSPs/GalacticMSPs.txt>

⁸ <http://www.naic.edu/~pfreire/GCpsr.html>

dense stellar environment the likelihood for the formation of binary systems is enhanced. This results in a higher probability to produce MSPs as it happens in the dense environment of globular clusters (Alpar et al. 1982; Verbunt & Hut 1987; Camilo et al. 2000). On the other hand, these MSPs might be the fossils of tidally disrupted globular clusters that fell in toward the Galactic center because of dynamical friction. They would release all their stellar content and contribute to the nuclear stellar cluster and the Galactic bulge (Tremaine et al. 1975; Arca-Sedda & Capuzzo-Dolcetta 2014; Gnedin et al. 2014; Brandt & Kocsis 2015).

A population of ~ 6000 MSPs at the Galactic center was first proposed by Wang (2005) in order to explain various multi-wavelength observations at the same time: the large number of unidentified *Chandra* X-ray sources (Muno et al. 2003), the EGRET GeV diffuse gamma-ray emission in the inner $1^\circ.5$ (Mayer-Hasselwander et al. 1998), and the TeV diffuse emission as measured by HESS (Aharonian et al. 2004) (see also Bednarek & Sobczak (2013) for interpretations of the TeV emission).

Lately, Abazajian (2011) proposed a population of MSPs associated with the bulge of the Galaxy as an explanation for the extended excess emission of GeV gamma-ray photons that has been found in observations of the inner Galaxy with the *Fermi* Large Area Telescope (LAT) (Hooper & Goodenough 2011; Vitale & Morselli 2009), dubbed the *Fermi* GeV excess. By now, numerous follow-up studies by several independent groups (Hooper & Linden 2011; Abazajian & Kaplinghat 2012; Gordon & Macias 2013; Abazajian et al. 2014; Daylan et al. 2016; Hooper & Goodenough 2014; Macias & Gordon 2014; Zhou et al. 2014; Calore et al. 2015b;), and lately also the LAT collaboration (Ajello et al. 2015), have confirmed the existence of this excess emission, which emerged above predictions from conventional Galactic diffuse emission models.

It is worth emphasizing that the word “excess” is somewhat misleading here, and potentially confusing. In fact, *none* of the Galactic diffuse emission models that were used in the above analyses actually included any realistic model for the gamma-ray emission of the Galactic bulge or center. Significant emission from the Galactic bulge hence necessarily shows up as “excess” above the model predictions. Since it is common in the literature, we will continue to refer to this emission as *Fermi* GeV excess, but note that a much more appropriate and descriptive term would be “Galactic bulge emission”.

The *Fermi* GeV excess shows specific spectral and spatial features (we follow here the results from Calore et al. (2015b) and note that Ajello et al. (2015) come to similar results where the analyses overlap). The best-fit to the energy spectrum is given by a broken power-law ($dN/dE \propto E^{-\alpha}$) with spectral indices $\alpha(E < E_b) = 1.4^{+0.2}_{-0.3}$ and $\alpha(E > E_b) = 2.6 \pm 0.1$, and a break energy of $E_b = 2.1 \pm 0.2$ GeV. However, power-laws with an exponential cutoff also fit the data well when taking into account the large systematic uncertainties related to the subtraction of Galactic diffuse foregrounds.⁹ This is in good agreement with the stacked spectrum of gamma-ray MSPs as determined by McCann (2015) (namely $E_{\text{cut}} = 3.6 \pm 0.2$ GeV and $\alpha = 1.46 \pm 0.05$; see Cholis et al. 2014 for similar results). Although the *Fermi* GeV excess is most clearly visible in the inner 5 deg of the Galactic center, indications for an

excess with a characteristic peak at around 2–3 GeV can be found up to 15 deg above and below the Galactic plane (Daylan et al. 2016; Calore et al. 2015b). The morphology of the excess is compatible with a spherical symmetric volume emissivity that is strongly peaked toward the Galactic center, and which follows a radial power-law of $d\mathcal{E}/dV \propto r^{-\Gamma}$, with $\Gamma = 2.56 \pm 0.20$ in the inner ~ 15 deg.

The energy spectrum of the *Fermi* GeV excess is indeed well in agreement with *Fermi* observations of Galactic field MSPs (Calore et al. 2015a). The combined emission from thousands of MSPs, too dim to be resolved by the telescope as individual objects, might produce the diffuse excess emission provided that the density of sources steeply rises toward the Galactic center (Abazajian 2011; Gordon & Macias 2013; Abazajian et al. 2014; Petrovic et al. 2014b; Yuan & Zhang 2014). Such an extended, spherically symmetric, spatial distribution could be generated as the debris from tidally disrupted globular clusters (Brandt & Kocsis 2015). Also, secondary gamma-ray emission can be produced from positron–electron pairs emitted by MSPs and up-scattering low-energy ambient photons up to ~ 100 GeV. Such emission could contribute to possible high-energy tails of the *Fermi* GeV excess (Petrovic et al. 2014b; Yuan & Ioka 2015).

Various other mechanisms have been proposed to account for or contribute to the *Fermi* GeV excess, and hence the gamma-ray emission from the Galactic bulge. Interestingly, the properties of the observed emission are compatible with a signal from the self-annihilation of dark matter particles in the dark matter halo of the Galaxy, see e.g. Calore et al. (2015b) and references therein. Other astrophysical scenarios that were discussed are leptonic outbursts of the supermassive black hole during an active past of the Galactic center (Carlson & Profumo 2014; Petrovic et al. 2014a; Cholis et al. 2015) and star formation activity in the central molecular zone (Carlson et al. 2015; Gaggero et al. 2015). However, a generic feature of models that explain the excess with inverse Compton emission of energetic leptons is that the excess spectrum should vary with distance from the Galactic center, which is not observed in the analysis of Calore et al. (2015b). Also, the observed excess morphology can only be accounted for with multiple finely tuned injection events (see Cholis et al. 2015 for details).

Recently, Bartels et al. (2015) and Lee et al. (2015) found an enhanced clustering of gamma-ray photons from the inner Galaxy, and showed that the most likely cause is contributions from a population of sources just below the detection threshold of *Fermi*. Furthermore, Bartels et al. (2015) showed that the inferred surface density and cutoff luminosity of the sub-threshold sources is compatible with the expectations from a bulge population of MSPs that can potentially account for 100% of the emission associated with the *Fermi* GeV excess. Significant contributions to the observed photon clustering from a thick-disk population of MSPs, extragalactic, or other Galactic sources were ruled out, and an un-modeled sub-structure in the gas emission seemed a rather unlikely cause. These results, together with the hard X-ray emission seen by *NuSTAR* (Perez et al. 2015), make the case for a population of MSPs at the Galactic center even stronger, and motivate additional multi-wavelength observation strategies to probe the MSP interpretation of the *Fermi* GeV excess.

Lastly, it is worth mentioning that the stacked spectral energy distribution (SED) of gamma-ray observed *young* pulsars, $P \geq 30$ ms and $B \geq 10^9$ G, is also in agreement with

⁹ $dN/dE \propto E^{-\alpha} \exp[-E/E_{\text{cut}}]$, with cutoff energy of $E_{\text{cut}} = 2.5^{+1.1}_{-0.8}$ GeV and a spectral index of $\alpha = 0.9^{+0.4}_{-0.5}$.

the spectral properties of the *Fermi* GeV excess. O’Leary et al. (2015) argued that a population of young pulsars arising from a star formation in the inner Galaxy and the kinematical evolution in the Galactic potential can account for most of the extended excess emission. However, this scenario does not account for the steep observed rise of the *Fermi* GeV excess toward the inner dozens of pc of the Galactic center (see, e.g., Daylan et al. 2016), and it seems to lead to an oblate rather than a spherical source distribution in the bulge. In the present work, we will hence assume that MSPs dominate the *Fermi* GeV excess. We note, however, the radio pulsation searches we investigate would also be at least equally sensitive to young pulsars, in addition to MSPs.

Despite considerable efforts, MSP searches in the Galactic center region have so far been unsuccessful. The main obstacles are the large scatter-broadening of the pulsed signal along the line of sight toward the inner Galaxy as well as the large distance to the sources. This prevents the detection of the pulsed radio emission in many cases (Stovall et al. 2013), because MSPs are generally weak radio sources (with flux densities in the range μJy to mJy). The only MSPs observed in the inner 3 kpc ($\sim 20^\circ$ at a distance of 8.5 kpc away) are MSPs associated with the globular clusters M62, NGC 6440, and NGC 6522, and were found in dedicated deep observations of these targets.

Finding the bulge source population at mid Galactic latitudes with multi-wavelength observations is certainly challenging. However, this possibility has never been systematically explored. Previous large radio surveys were shown to be insensitive to MSPs at the Galactic center (Macquart & Kanekar 2015). Moreover, those same surveys were focused on the very inner few degrees about the Galactic center, while, supported by the diffuse gamma-ray emission, we expect the bulge MSP population to extend to latitudes of about $\pm 15^\circ$.

In this paper we analyze the prospects for the detection of a bulge MSP population (as suggested by the *Fermi* GeV excess) via searches for radio pulsations. One of the most detailed descriptions of the *Fermi* GeV excess at $|b| > 2^\circ$ latitudes was presented by Calore et al. (2015b), and we will base our modeling on these results. We discuss various radio survey strategies that could unveil the bulge MSP population with existing and future instruments. To this end, we will use observations of globular clusters as well as high-latitude gamma-ray MSPs and unassociated *Fermi* sources to calibrate our predictions.

The paper is organized as follows: in Section 2 we describe the modeling we adopt for the bulge MSP population, as motivated by the observation of the GeV excess, and its radio luminosity function. In Section 3 we estimate the sensitivity of current and future radio instruments to MSP detection. We present our results for large area radio surveys in Section 4. In Section 5 we study the possibility of detecting the bulge sources in deep targeted observations by exploiting an observed loose correlation between gamma-ray and radio fluxes. We discuss various additional aspects and caveats of our results in Section 6, where we also briefly comment on the possibility to use X-rays to probe the bulge MSP population. We conclude in Section 7.

In the Appendix we further investigate the MSP candidates identified by Bartels et al. (2015) as significant wavelet peaks in gamma-ray data from the inner Galaxy. In particular, we

look for a possible correlation of wavelets peaks with foreground sources, i.e., MSPs or young pulsars along the line of sight but closer to us than bulge MSPs. Finally, we provide a multi-wavelength analysis of the 13 MSP candidates from Bartels et al. (2015).

2. MODELING THE BULGE MSP POPULATION

We start by constructing a phenomenological model for the radio emission properties of the bulge MSP population as a whole. The aim is to obtain a reliable estimate for the surface density of *radio-bright* MSPs in the Galactic bulge. To this end, we define *radio-bright* as any MSP that has a period-averaged flux density of at least $10 \mu\text{Jy}$ at 1.4 GHz. This is rather low compared to values that are conventionally used in the literature, but will turn out to be appropriate for the discussion in this work and is motivated by the sensitivities of currently available radio telescopes.

We assume that bulge MSPs are responsible for the dominant part of the *Fermi* GeV excess (hence the dominant part of the Galactic bulge emission), and we will adopt below a spatial distribution that is consistent with *Fermi*-LAT observations. We adopt here a phenomenological approach to the problem; we do not pretend to fully model the dynamics and evolution of the Galactic bulge, but we assume the spatial distribution required to explain the *Fermi* GeV excess data. Once the spatial distribution is fixed, however, estimating the number of radio-bright MSPs in the bulge from diffuse gamma-ray observations is rather challenging at first sight. One would expect that it requires accurate information about both the gamma-ray and radio luminosity functions, and a detailed understanding of beaming effects. However, the discussion is greatly simplified for the specific goals of this paper, as we shall see next.

In most of the current paper we are interested in the *combined* gamma-ray emission of many bulge MSPs (averaged over regions of, say, 1 deg^2). This is what we can actually most readily determine with *Fermi*-LAT observations in contrast to the much harder to detect the gamma-ray emission of individual bulge sources. Details of the gamma-ray luminosity function, and the potential correlation of the gamma-ray with radio emission on a source-by-source basis, are not directly relevant when studying the average emission properties of MSPs in the Galactic bulge. They will only become relevant when discussing targeted observations in Section 5 below.

For our predictions we need for a given random sample of N_{tot} MSPs at the distance of the Galactic bulge:

- A. An estimate for the number of radio-bright MSPs in that population, N_{rb} .
- B. An estimate for their combined gamma-ray emission, L_γ .

Since our predictions for the number of radio-bright MSPs in the bulge will only depend on the ratio N_{rb}/L_γ , the total number, N_{tot} , will drop out.

The predictions in this paper rely on two critical assumptions.

(1) We will assume that both the population of bulge MSPs and of MSPs bound in globular clusters have similar gamma-ray and radio emission properties. This is justified by the fact that—while the formation of MSPs in globular clusters versus the field may in some cases follow different paths—the fundamental physical processes creating the observed radio

Table 1
List of Globular Clusters that We Use as a Proxy for the Population of Bulge MSPs

Globular cluster	ℓ (deg)	b (deg)	d (kpc)	L_γ (10^{34} erg s^{-1})	N_{obs}	N_{rad}
Ter 5	3.8	1.7	5.5	26.5 ± 9.0	25	82 ± 16
47 Tuc	305.9	-44.9	4.0	5.1 ± 1.1	14	37 ± 10
M 28	7.8	-5.6	5.7	6.4 ± 2.0	9	63 ± 21
NGC 6440	7.7	3.8	8.5	35.4 ± 8.0	6	48 ± 21
NGC 6752	336.5	-25.6	4.4	1.3 ± 0.7	5	21 ± 10
M 5	3.9	46.8	7.8	2.4 ± 0.5	5	13 ± 6
Stacked				77.1 ± 12.3	64	264 ± 37

Note. We show name, galactic longitude and latitude, distance, gamma-ray luminosity (Acero et al. 2015; Zhou et al. 2015), the number of observed radio MSPs relevant to this work (N_{obs}), and the estimated *total* number of radio MSPs (N_{rad}), based on our reference radio luminosity function. Furthermore, in the last row, we show the *stacked* gamma-ray luminosity ($L_\gamma^{\text{stacked}}$) and the estimated number of radio MSPs ($N_{\text{rad}}^{\text{stacked}}$). If not otherwise stated, parameters are taken from Bagchi et al. (2011), Model 3. Note that N_{obs} refers to the number of observed MSPs with quoted flux densities that were used in Bagchi et al. (2011) to infer the radio luminosity function.

pulsations should in all cases be the same. At the same time, globular cluster and field MSPs do not have obvious age differences or luminosity distributions (Konar 2010). Thus, we can use the gamma-ray emission from globular clusters as well as the radio observations of MSPs in globular clusters as a proxy for the population of bulge MSPs.

(2) We assume that *all* of the gamma-ray emission from globular clusters comes from MSPs. If only a fraction f_{MSP} of the gamma-ray emission came from MSPs this would simply *increase* the number of radio-bright MSPs in the bulge by a factor of $\propto f_{\text{MSP}}^{-1}$ with respect to our predictions below. Therefore, this is a conservative assumption.

2.1. Lessons from MSPs in Globular Clusters

To estimate the number of radio-bright sources expected from a population of MSPs located at the GC (A) we will use the radio luminosity function of detected globular clusters (Bagchi et al. 2011) and rescale it to a distance of 8.5 kpc. We will assume their combined gamma-ray luminosity (B) by stacking the measured *Fermi* gamma-ray fluxes of the globular clusters in our sample. We will use the ratio between the stacked gamma-ray emission from globular clusters and the expected number of radio-bright MSPs (at 8.5 kpc) as a proxy for the relationship between the mean gamma-ray luminosity and the mean number of radio-bright MSPs in the Galactic bulge (see details below). In this way, we will be able to get a robust estimate for the number of radio-bright MSPs in the Galactic bulge.

In Table 1 we list the globular clusters that we take into account in the present discussion. This is the subset of objects considered in Bagchi et al. (2011) for which gamma-ray measurements exist. The number of detected radio MSPs in the globular clusters in Table 1 is relatively large, ranging from five sources in NGC 6752 and M 5, to 25 sources in Terzan 5 (note that actually 33 MSPs with $P < 30$ ms are known in Terzan 5, but only 25 were taken into account in the study of Bagchi et al. 2011). We note that Terzan 5 and NGC 6440 are the most luminous gamma-ray emitters, and we discuss their role for our results below.

The total number of radio MSPs, N_{rad} , in each globular cluster can be estimated by a fit of a given radio luminosity function (with free normalization but fixed shape) to the globular cluster MSPs that are individually detected in the radio. The radio luminosity function of globular cluster MSPs was studied in great detail by Bagchi et al. (2011), using Monte

Carlo techniques that account for the finite observation depths.¹⁰ They found that the cumulative radio luminosity function of MSPs in globular clusters is similar to the luminosity function of young and recycled pulsars in the disk as derived by Faucher-Giguère & Kaspi (2006).

We will adopt here the best-fit model from Bagchi et al. (2011) (their “Model 3”) as a reference for the radio luminosity function. In Section 6 we will comment on how our results depend on that choice. The luminosity function follows parametrically a log-normal distribution,

$$f(L_\nu) = \frac{\log_{10} e}{L_\nu} \frac{1}{\sqrt{2\pi\sigma^2}} \exp\left[-\frac{(\log_{10} L_\nu - \mu)^2}{2\sigma^2}\right], \quad (1)$$

with mean $\mu = -0.52$ and variance $\sigma = 0.68$, and L_ν refers to the “pseudo-luminosity” at $\nu = 1.4$ GHz (mJy kpc^2). The pseudo-luminosity is related to the measured flux density, S_ν , of a source by $L_\nu = S_\nu d^2$, where d denotes the distance to the source. It is used because the beaming angle of the radio emission is unknown.

Note that the above radio luminosity function has a high-luminosity tail that predicts sources brighter than the brightest MSPs detected so far in globular clusters (where the distance is relatively well known). In order not to unrealistically bias our prediction toward excessively bright sources, we truncate the radio luminosity function to a maximum pseudo-luminosity of 30 mJy kpc^2 . Such a pseudo-luminosity corresponds to the maximum flux density, 0.4 mJy , observed in stacked globular clusters rescaled to a distance of 8.5 kpc, cf. Figure 1.¹¹

Based on the radio luminosity function in Equation (1), the number of radio MSPs in each globular cluster was inferred by Bagchi et al. (2011). The results, together with 1σ error bars from the fits, are listed in Table 1. In this table we also show the total number of radio MSPs in all considered globular clusters combined. It is $N_{\text{rad}}^{\text{stacked}} = 264 \pm 37$ (with errors summed in quadrature). We note that the *total* number of MSPs in the globular clusters are definitively larger, since not all MSPs are expected to have a radio beam pointing toward the Earth

¹⁰ Note that although the study formally takes into account all pulsars in globular clusters, the sample that they use is completely dominated by MSPs.

¹¹ We also point out that there are only a handful of MSPs in the ATNF catalog that have a pseudo-luminosity at 1.4 GHz higher than 30 mJy kpc^2 . These have pseudo-luminosities of about 50–60 mJy kpc^2 , with one exceptional source at B1820-30A at 100 mJy kpc^2 .

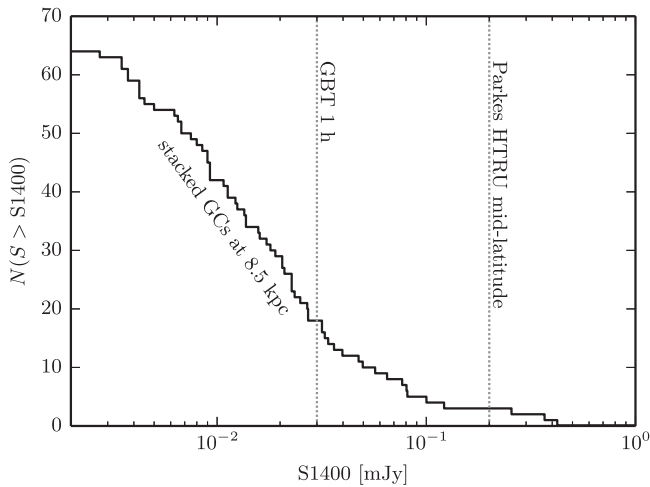


Figure 1. Complementary cumulative distribution of flux densities at 1.4 GHz, S1400, of the 64 pulsars in the globular clusters that are listed in Table 1, rescaled to a distance of 8.5 kpc. We show for comparison the limiting flux density, ~ 0.2 mJy, of the Parkes High Time Resolution universe (HTRU) mid-latitude survey (Keith et al. 2010) as well as the reference GBT survey, 0.03 mJy (discussed in Section 3). The plot illustrates that a survey that is significantly deeper than that with Parkes would start probing the radio luminosity function in a regime that is well supported by data. Predictions for *radio-bright* bulge MSPs ($S1400 \geq 10 \mu\text{Jy}$) are built upon 43 measured globular cluster MSPs.

(although the beams are arguably wide in the case of MSPs); this, however, is not relevant for our discussion.

It is reassuring that, for a bulge population of MSPs, measuring flux densities below 0.1 mJy (at 1.4 GHz) is enough to start probing the parts of the radio luminosity function that are directly supported by observations (rather than by an extrapolation beyond the brightest observed MSP). To illustrate this point, we rescale the flux densities of MSPs observed in the globular clusters from Table 1 to the distance of the Galactic center, for which we here adopt 8.5 kpc (consistent with Gillissen et al. 2009). We show the resulting complementary cumulative distribution function of these flux densities in Figure 1. In this figure we also indicate, for comparison, the maximum sensitivity of our reference Parkes and GBT observations from Table 3, which we will discuss in detail below.

Lastly, in Table 2, we indicate the number of *radio-bright* MSPs in the stacked globular clusters, assuming that they are at a distance of 8.5 kpc.¹² To this end, we use our above reference luminosity function normalized to the number of radio pulsars as indicated in Table 1, but we also show results for the two other luminosity functions from Bagchi et al. (2011) which reasonably bracket the uncertainties implied by the observed MSPs (see their Figure 3). We find that, although the *total* number of radio MSPs (which is just obtained by integrating the appropriately normalized radio luminosity function to the lowest luminosities) is uncertain by at least a factor of a few, the number of *radio-bright* MSPs is much better constrained, since it has direct observational support. Indeed, this is also apparent from Figure 1 above.

¹² We note that the number of radio-bright sources in Figure 1, which is based on various flux-limited samples that were used in the analysis by Bagchi et al. (2011), is, as expected, somewhat smaller than the corresponding values quoted in Table 2 that were obtained from the inferred luminosity functions.

Table 2

Estimated Total Number of Radio MSPs ($N_{\text{rad}}^{\text{stacked}}$) and of Radio-Bright MSPs ($N_{\text{rb}}^{\text{stacked}}$) in the Stacked Globular Clusters from Table 1, as Inferred from the Observed MSPs Using Three Different Luminosity Functions (Bagchi et al. 2011, Their Models 1–3)

Luminosity function (μ, σ)	$N_{\text{rad}}^{\text{stacked}}$	$N_{\text{rb}}^{\text{stacked}}$ ($d \simeq 8.5$ kpc)
Model 1 (−1.1, 0.9)	514 ± 71	74 ± 10
Model 2 (−0.61, 0.65)	339 ± 49	80 ± 12
Model 3 (−0.52, 0.68)	264 ± 37	76 ± 11

Note. Reference luminosity function used in most of this paper is *Model 3*. We assume the MSPs are at a distance of 8.5 kpc (i.e., at the galactic center) in order to determine whether they are radio-bright. We find that, while the estimated *total* number of radio MSPs in the stacked globular clusters depends on the rather uncertain low-luminosity tail of the radio luminosity function, the estimated number of MSPs that we would qualify as radio-bright remains consistent within the error bars for all the three models.

The total gamma-ray luminosity from all considered globular clusters combined is $L_{\gamma}^{\text{stacked}} = (7.71 \pm 1.23) \times 10^{35} \text{ erg s}^{-1}$, where the error refers to *Fermi* flux measurement errors that are added in quadrature. The stacked luminosity is dominated by Terzan 5 and NGC 6440, and we refer to Section 6 for further discussions about the effect of individual globular clusters on our results. Following Abdo et al. (2013), we define gamma-ray luminosity as $L_{\gamma} = 4\pi d^2 G_{100}$, where G_{100} is referring to the energy flux measured by *Fermi*-LAT above 100 MeV.

Gamma-ray luminosity functions have, in general, very non-Gaussian tails, and one might worry that the sample variance of the combined gamma-ray emission of the six globular clusters is excessively large. We estimate the sample variance of this summed gamma-ray luminosity in a simple toy scenario. To this end, and *only* for the purpose of estimating the variance, we assume that the summed gamma-ray emission of the globular clusters is caused by about 250 MSPs that are randomly drawn from a power-law gamma-ray luminosity function with hard lower and upper cutoffs at $10^{32} \text{ erg s}^{-1}$ and $10^{35} \text{ erg s}^{-1}$, respectively. The upper cutoff is selected to be compatible with the brightest observed MSPs, the lower cutoff is adjusted such that 250 sources yield the combined total luminosity. The index of the luminosity function is fixed to -1.5 (see discussions in Cholis et al. 2014; Petrovic et al. 2014b; Strong 2007; Venter et al. 2014). We find a mean total luminosity of $7.9 \times 10^{35} \text{ erg s}^{-1}$, comparable to the above value for $L_{\gamma}^{\text{stacked}}$, and the standard deviation of the total luminosity over many samples is $1.5 \times 10^{35} \text{ erg s}^{-1}$. This implies that $L_{\gamma}^{\text{stacked}}$ can be considered as a reasonable estimate for the population averaged gamma-ray luminosity, with a sample variance uncertainty of about 20%. Indeed, this is larger than the 6% that would be expected from shot noise alone for a population with an average number of 250 sources. We will adopt the 20% here as an estimate for the sample variance, but we stress that the precise value depends on the not well-constrained details of the gamma-ray luminosity function at high luminosities.

We now calculate the ratio between the overall gamma-ray emission from globular clusters and the number of radio-bright MSPs (assuming 8.5 kpc distance), taking into account uncertainties in the number of total radio MSPs, *Fermi* flux measurements and sample variance. We will subsequently assume that this ratio provides the relationship between the mean gamma-ray luminosity ($\langle L_{\gamma}^{\text{bulge}} \rangle$) and the mean number of

radio-bright MSPs ($N_{\text{rb}}^{\text{bulge}}$) in the Galactic bulge. It is given by

$$\mathcal{R}_{\text{rb}}^{\gamma} \equiv \frac{\langle L_{\gamma}^{\text{bulge}} \rangle}{\langle N_{\text{rb}}^{\text{bulge}} \rangle} \simeq \frac{L_{\gamma}^{\text{stacked}}}{N_{\text{rb}}^{\text{stacked}}} = (1.0 \pm 0.3) \times 10^{34} \text{ erg s}^{-1}. \quad (2)$$

We emphasize that the value of $\mathcal{R}_{\text{rb}}^{\gamma}$ does *not* provide a robust estimate for the average gamma-ray luminosity of radio-bright MSPs, since not every gamma-ray emitting MSP must be bright in radio or vice versa. But it provides a reasonable relation between the overall gamma-ray luminosity of a large population of MSPs and the number of radio-bright sources in that same population at Galactic center distances.

The errors that we quote for $\mathcal{R}_{\text{rb}}^{\gamma}$ do not directly take account the effect of varying the radio luminosity function. However, as we discussed above and showed in Table 2, the systematic uncertainties related to the adopted luminosity function are smaller than the statistical error from fitting the luminosity function to the globular cluster observations. Given this, and the various other uncertainties that enter the estimate in (2), these variations can be neglected.

As we will see, the spin period is critical for the detectability of MSPs. The analysis of the spin period distribution of field MSPs by Lorimer et al. (2015) finds a modified log-normal distribution. The mean is $P_{\text{mean}} \simeq 5.3$ ms and hence in good agreement with the mean of the observed periods of MSPs in globular clusters ($P_{\text{mean}} \simeq 5.7$ ms) (Konar 2010). We will use here the results from Lorimer et al. (2015) as reference.

2.2. Predicted Radio-bright MSPs in the Galactic Bulge

Following the results of the gamma-ray analysis by Calore et al. (2015b), we assume that the density of field MSPs in the Galactic bulge follows an inverse power-law as function of the Galacto-centric distance, r , with an index of $\Gamma = 2.56$. For definiteness, we adopt a hard cutoff at $r = 3$ kpc, which is not critical for our results. We fix the normalization of the combined (and population averaged) gamma-ray intensity of this bulge population in the pivot direction $(\ell, b) = (0^{\circ}, \pm 5^{\circ})$. In this direction, and for a reference energy of $E_{\gamma} = 2$ GeV, the differential intensity of the proposed bulge MSP population is given by $\Phi = (8.5 \pm 0.7) \times 10^{-7} \text{ GeV}^{-1} \text{ cm}^{-2} \text{ s}^{-1} \text{ sr}^{-1}$ (Calore et al. 2015b). We remark that the quoted gamma-ray intensity is not the *total* intensity of the excess emission (which is to some degree ill-defined, given the large uncertainties in the Galactic diffuse foregrounds) but the fraction that can be reasonably attributed to MSP-like spectra after accounting for foreground subtraction systematics (for details see Calore et al. 2015b).

We assume that the energy spectrum of the combined gamma-ray emission of bulge MSPs follows the stacked MSP spectrum inferred by McCann (2015) from 39 nearby sources. As mentioned in the introduction, this spectrum is in good agreement with the spectrum of the *Fermi* GeV excess as derived by Calore et al. (2015b). The above differential intensity at 2 GeV corresponds, then, to an energy intensity (above 100 MeV) of $(5.5 \pm 0.5) \times 10^{-12} \text{ erg cm}^{-2} \text{ s}^{-1} \text{ deg}^{-2}$. Using the ratio $\mathcal{R}_{\text{rb}}^{\gamma}$ as estimated in the previous subsection, this implies a surface density of radio-bright bulge MSPs at five degrees above and below the Galactic center of around $(4.7 \pm 1.5) \text{ deg}^{-2}$.

With the above assumptions, we find a total gamma-ray luminosity of the MSP bulge population of

$$L_{\gamma}^{\text{bulge}} = (2.7 \pm 0.2) \times 10^{37} \text{ erg s}^{-1}. \quad (3)$$

We note that variations of the spatial index, Γ , by ± 0.2 , which is the 1σ range found in Calore et al. (2015b), would affect the total gamma-ray luminosity by up to 40%. However, we do not propagate this additional uncertainty through the analysis, because most of our conclusions will depend on the emission around the above-mentioned pivot directions, which makes them relatively independent on the exact value of Γ .

Using the ratio $\mathcal{R}_{\text{rb}}^{\gamma}$ as estimated in the previous subsection, we obtain *an estimate for the number of radio-bright MSPs in the Galactic bulge*,

$$N_{\text{rb}}^{\text{bulge}} = (2.7 \pm 0.9) \times 10^3. \quad (4)$$

As discussed above in the context of Table 2, the number of radio-bright sources is relatively weakly dependent on the adopted radio luminosity function. However, when simulating sources in the Galactic bulge we actually need the number of all radio MSPs. We will, in the remaining part of the paper, adopt ‘‘Model 3,’’ for which we find a total number of radio MSPs of $N_{\text{rad}}^{\text{bulge}} = (9.2 \pm 3.1) \times 10^3$. About 1/3 of the radio MSPs are thus radio-bright, i.e., $\geq 10 \mu\text{Jy}$.

2.3. Comparison with the MSP Thick-disk Population

We illustrate the putative bulge population of radio MSPs in Figure 2. There we show the distribution of bulge radio MSPs in Galacto-centric Cartesian coordinates, both in x - z and x - y projection, and compare it with the actually observed MSPs and with a thick-disk MSP population (Faucher-Giguère & Loeb 2010). We assume that the population of thick-disk MSPs has a cylindrical symmetry with an exponential distribution, and with a scale radius of 5 kpc (Faucher-Giguère & Loeb 2010) and a scale height of 0.5 kpc (Calore et al. 2014; Lorimer et al. 2015). Following Levin et al. (2013), we attribute 20,000 radio MSPs to the disk. We note that in this way we will somewhat over-predict the number of pulsars detectable with the Parkes HTRU (as discussed below in Section 6). This is, however, not critical for our results, since having a smaller number of thick-disk sources would make the bulge component even more pronounced.

Analogously to the bulge MSP population, the radio luminosity function of disk MSPs is modeled according to our reference radio luminosity function. From Figure 2 it is very clear that the observed spatial distribution of *known* MSPs is almost exclusively driven by selection effects that limit the maximum distance to which they can be found, and should obviously not be used as a proxy for the real distribution of MSPs in the Galaxy.

Lastly, the implied *surface density* of radio-bright bulge MSPs is shown in Figure 3. At $(\ell, b) = (0^{\circ}, \pm 5^{\circ})$ it is consistent with our above simple estimate (although we now take into account the varying distances to the bulge sources that can be slightly closer or further away than 8.5 kpc depending on their position). Otherwise, it ranges from >300 sources deg^{-2} around the Galactic center to just a hand full of sources deg^{-2} a few degrees away from the Galactic center.

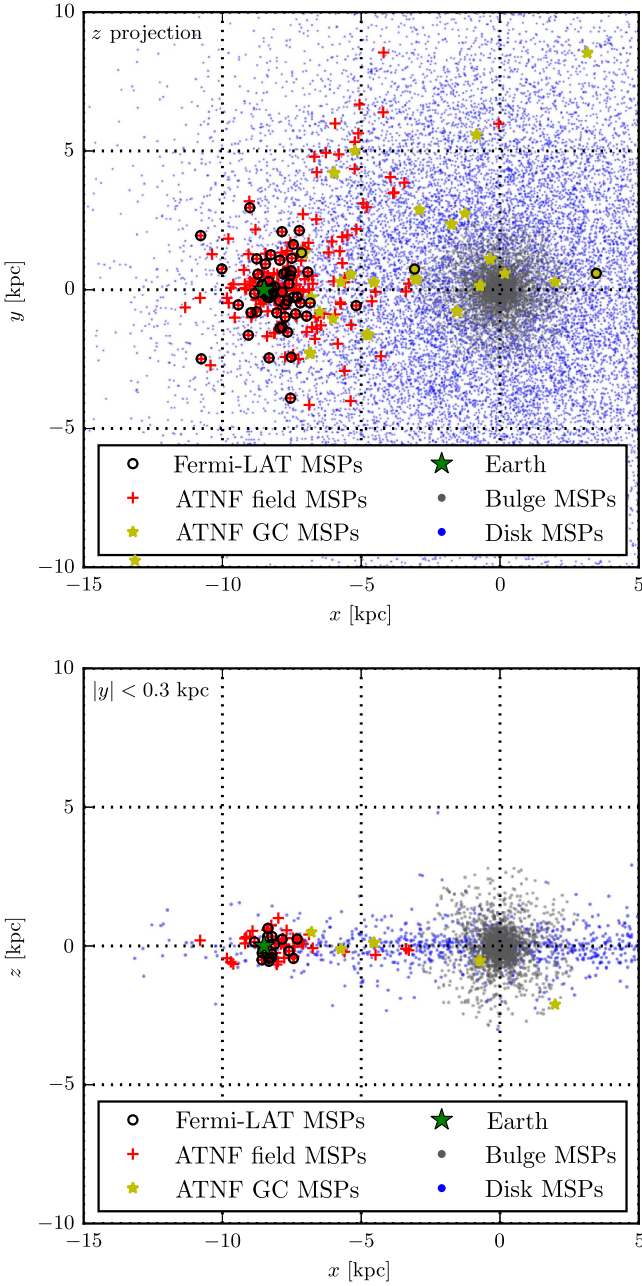


Figure 2. Predicted spatial distribution of MSPs in the bulge (*gray dots*) and the disk (*blue dots*) modeled based on gamma-ray and radio data as we describe in the text. For comparison, we also show the position of measured radio pulsars with $P < 30$ ms from the Australia Telescope National Facility (ATNF) catalog, both sources in the field (*red crosses*) and MSPs in globular clusters (*yellow stars*). We also show gamma-ray detected field MSPs (*black circles*). Distance estimates for these sources are based on the NE2001 model (Cordes & Lazio 2002), except for globular clusters where distances are better known and taken from the ATNF. We show projections both in the x - y (*upper panel*) and the x - z plane (*lower panel*), and mark the position of the Earth (in our convention at $z = y = 0$ and $x = -8.5$ kpc). In the lower panel, we only show a thin slice with $|y| < 0.3$ kpc in order to better visualize the increased source densities in the inner Galaxy.

3. SENSITIVITY OF RADIO TELESCOPES

Here, we summarize briefly how we estimate the sensitivity of radio pulsation searches.

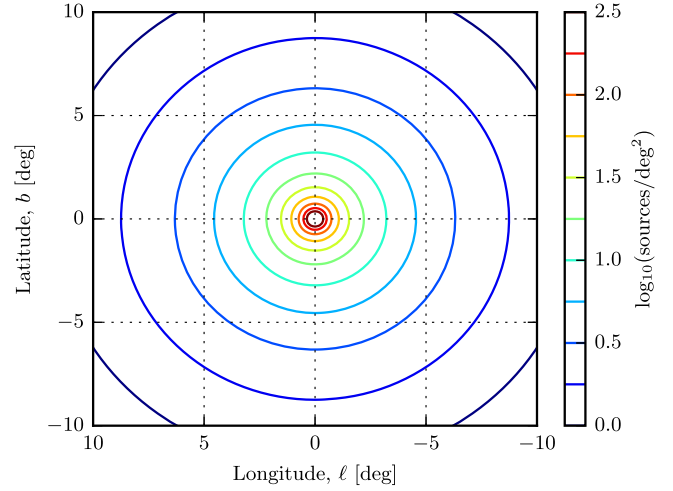


Figure 3. Surface density of radio-bright (i.e., $\geq 10 \mu$ Jy) bulge MSPs toward the inner Galaxy, per deg^2 . Beyond an angular distance of 5° from the Galactic center, the density drops well below $\sim 5 \text{ deg}^{-2}$.

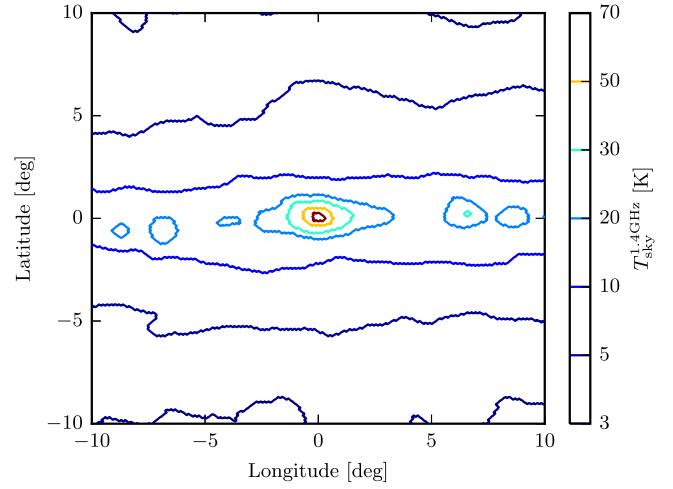


Figure 4. Sky temperature contours at 1.4 GHz, $T_{\text{sky}}^{1.4\text{GHz}}$ (K), as derived from the Haslam 408 MHz radio maps (Haslam et al. 1982). The strong emission in the Galactic disk and Galactic center increases the background noise for MSP searches in these regions by a factor of a few. Note that point sources are not removed and affect our results close to the Galactic center.

3.1. Radiometer Equation

From the radiometer equation (see e.g. Dewey et al. 1984), the rms uncertainty of the flux density (in mJy) is given by

$$S_{\nu,\text{rms}} = \frac{T_{\text{sys}}}{G \sqrt{t_{\text{obs}} \Delta\nu n_p}} \left(\frac{W_{\text{obs}}}{P - W_{\text{obs}}} \right)^{1/2}, \quad (5)$$

where $T_{\text{sys}} = T_{\text{sky}} + T_{\text{rx}}$ is the system temperature (K) given by the sum of the sky and receiver temperatures, G is the telescope gain (K Jy^{-1}), n_p is the number of polarizations, $\Delta\nu$ is the frequency bandwidth (MHz), and t_{obs} is the integration time (s). The sky temperature is a function of Galactic longitude and latitude. For any given line of sight we compute the corresponding sky temperature from the Haslam 408 MHz all-sky radio maps (Haslam et al. 1982), assuming a power-law rescaling to the frequency of interest with index -2.6 (Lawson et al. 1987). In Figure 4 we show the contours of constant T_{sky}

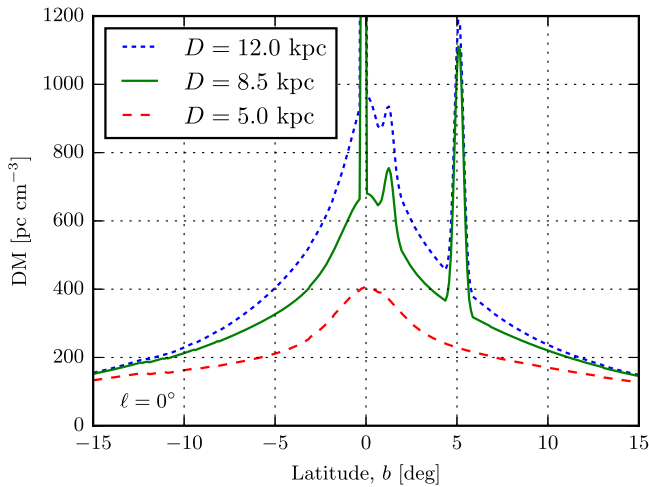


Figure 5. Latitude dependence of dispersion measure, DM, as derived from the NE2001 model (Cordes & Lazio 2002), at zero Galactic longitude, $\ell = 0^\circ$, for different line of sight distances between $D = 5$ kpc and $D = 12.0$ kpc. At longitudes in the range $\ell = [-10^\circ, 10^\circ]$ the values typically differ by $<10\%$. The spikes in the otherwise smooth curves correspond to discrete “clumps” of enhanced free electron density that are included in the NE2001 model (see Tables 5–7 in Cordes & Lazio 2002).

for a $20^\circ \times 20^\circ$ region around the Galactic center at 1.4 GHz. As for the gain, the sensitivity calculations here assume an effective estimate that accounts for the fact that the gain decreases by a factor of two toward the FWHM edge of the telescope beam. This effect should be taken into account when planning actual surveys.

A reliable, blind pulsar detection requires a signal flux density of $S_\nu \geq 10 \times S_{\nu,\text{rms}}$. In order to detect the pulsations, the observed (or effective) pulse width, W_{obs} (ms), should be small with respect to the source period, P (ms). The observed pulse width can be estimated as (e.g., Hessels et al. 2007):

$$W_{\text{obs}} = \sqrt{(w_{\text{int}}P)^2 + \tau_{\text{DM}}^2 + \tau_{\text{scatt}}^2 + \tau_{\text{samp}}^2 + \tau_{\Delta\text{DM}}^2}, \quad (6)$$

where $w_{\text{int}} \sim 0.1$ is the intrinsic fractional pulse width typical for MSPs, τ_{DM} is the dispersive smearing across an individual frequency channel that depends on the dispersion measure (DM) of the source, τ_{scatt} is the temporal smearing due to multipath propagation from scattering in a non-uniform and ionized interstellar medium, τ_{samp} corresponds to the data sampling interval, and $\tau_{\Delta\text{DM}}$ is the smearing due to finite DM step size in the search. We note that typically intra-channel smearing, τ_{DM} , can be mostly ignored as long as one assumes that the data is taken with a high-enough frequency resolution. Here we model the intra-channel smearing as τ_{DM} is related to the DM, $\tau_{\text{DM}} = 8.3 \times 10^6 \text{ DM } \Delta\nu_{\text{chan}}/\nu^3$, where $\Delta\nu_{\text{chan}}$ is the channel bandwidth, i.e., the total bandwidth divided by the number of channels (Hessels et al. 2007). Throughout we also neglect $\tau_{\Delta\text{DM}}$, since sufficiently small DM step sizes can make this contribution small as well. The only limitation comes from the computing resources that are available for the problem (besides, of course, temporal smearing).

The dispersion measure, DM, which enters in the definition of both τ_{DM} and τ_{scatt} , for any given line of sight and distance of the source is computed using the Cordes-Lazio model for free

electron density in the Galaxy, NE2001 (Cordes & Lazio 2002).¹³ In Figure 5 we show the latitude profile of the DM, as derived from Cordes & Lazio (2002), for $\ell = 0^\circ$ and for different distances of the source from the Galactic center. The scattering time is modeled according to Bhat et al. (2004). We adopt a log-normal distribution with mean $\mu = \log_{10} \tau_{\text{scatt}}$, and a variance $\sigma = 0.8$ is assumed to account for the large uncertainty affecting τ_{scatt} . Indeed, while DM just depends on the column density of free electrons, the amount of scattering depends on how these electrons are distributed along the line of sight. Note that, typically, temporal scattering has the effect of smearing out the radio pulsations of almost all MSPs within a degree of the Galactic disk to the point of undetectability—for the assumed observing frequency of 1.4 GHz. Unlike dispersive broadening, it is not possible to correct the measurement for scattering broadening, which is thus a fundamental limit for detection.

We note that, since most MSPs are found in binary systems, the effect of Doppler smearing due to orbital motion also has a significant impact on the ability to blindly detect new pulsars. This is particularly true for the shortest (a few hours) orbital periods and most massive companions (Ransom 2001).

3.2. Instrumental Parameters

In the present work we provide the predicted yields of bulge MSPs for three observational scenarios based on the performances of currently operating and upcoming radio telescopes: GBT, MeerKAT, and SKA-mid. As a reference, and for comparison with past results, we choose to present results for surveys at 1.4 GHz. This turns out to be close to optimal in many cases, and we discuss how our sensitivity predictions change at higher and lower frequencies in Section 6. In Table 3 we quote the parameters used for each instrument. Parameters for the GBT are based on the GUPPI back-end and taken from the Proposer’s Guide for the GBT.¹⁴ Sensitivities for the future MeerKAT and SKA-mid are based on the SKA Phase 1 System Baseline Design report.¹⁵ We implement the performances of the MeerKAT and of the SKA-mid (350–3050 MHz) Antenna Array configuration. The quoted antenna gain in Table 3 ($G = T_{\text{sys}}/\text{SEFD}$) is derived from the system-equivalent flux density (SEFD) assuming a receiver temperature of 25 K (for the specific purpose of deriving the antenna gain from published results we here neglect the sky temperature, however we do fully account for it when deriving the sensitivity predictions.) For other parameters entering in Equation (6), such as the number of channels and the sampling interval, we refer to the corresponding values quoted for each telescope in the references provided above. As for GBT, we use a sampling time of $41 \mu\text{s}$ and 2048 channels. We emphasize that our estimates for MeerKAT and SKA-mid are only of indicative value, and should be updated once these telescopes are operational and accurate telescope performance parameters are known. Furthermore, the amount of data that can be collected with these instruments in a short time is enormous, and the likely bottleneck for pulsar searches will be the available computer processing resources for exploring the full telescope field of view and relevant astrophysical parameter

¹³ <http://www.nrl.navy.mil/rsd/RORF/ne2001/>

¹⁴ <https://science.nrao.edu/facilities/gbt/proposing/GBTpg.pdf>

¹⁵ http://www.skatelescope.org/wp-content/uploads/2012/07/SKA-TEL-SKO-DD-001-1_BaselineDesign1.pdf, see Table 1.

Table 3

Relevant Instrumental and Observational Parameters for Existing (Parkes HTRU, GBT) and Future (MeerKAT, SKA-Mid) Telescopes that we Consider in this Work. Where Possible, Values are Taken from Table 1 of the SKA Baseline Design Report

Parameters	HTRU (mid)	GBT	MeerKAT	SKA-mid
ν (GHz)	1.35	1.4	1.4	1.67
$\Delta\nu$ (MHz)	340	600	1000	770
t_{samp} (μs)	64	41	41	41
$\Delta\nu_{\text{chan}}$ (kHz)	332	293	488	376
T_{rx} (K)	23	23	25	25
G (K Jy^{-1})	0.74	2.0	2.9	15
Max. Base. Used (km)	—	—	1.0	0.95
Eff. G sub-array (K Jy^{-1})	0.74	2.0	2.0	8.5
Ele. θ_{FWHM} (arcmin)	14	8.6	65	49
Ele. FoV (deg^2)	0.042	0.016	0.92	0.52
Beam θ_{FWHM} (arcmin)	14	8.6	0.88	0.77
Beam FoV (deg^2)	0.042	0.016	0.00017	0.00013
# Beams	13	1	3000	3000
Eff. FoV (deg^2)	0.55	0.016	0.51	0.39
T_{point} (minute)	9	20	20	20
$T_{108 \text{ deg}^2}$ (hr)	29	2250	71	92
# Bulge(Fore-ground) MSPs	1(6)	34(37)	40(41)	207(112)

Note. We quote the survey central observing frequency, ν ; effective bandwidth, $\Delta\nu$; sampling time, t_{samp} ; channel bandwidth, $\Delta\nu_{\text{chan}}$; receiver temperature, T_{rx} ; gain of the whole array G ; maximum baseline used (where applicable), “Max. Base. Used”; the effective gain of the sub-array that can be used for wide-field pulsar surveys, “Eff. G sub-array”; the beam-width of the elements in the array, “Ele. θ_{FWHM} ”; the field of view of the array elements, “Ele. FoV”; the beam-width of the synthesized beam, beam θ_{FWHM} ; the field of view of the synthesized beam, “Beam FoV”; the number of beams recorded per pointing, “# Beams”; and the effective field of view per pointing, “Eff. FoV.” Next we give the integration time per pointing, the time required to cover 108 deg^2 of sky, and the total expected yield of bulge and foreground MSPs from a region of that size. The target region is here defined as ($|\ell| < 5^\circ$ and $3^\circ < |b| < 7^\circ$). Plus ($|\ell| < 3^\circ$ and $1^\circ < |b| < 3^\circ$) plus ($|\ell|, |b| < 1^\circ$).

space. Since not all data can be stored and analyzed offline, our estimated observation times for MeerKAT and SKA-mid are almost certainly too optimistic, probably by a factor of a few. In the same way, we assume that the entire arrays are used in the search. However, when doing the measurement, only a limited baseline (and hence only a subset of the full array) should be used in order to increase the size of the synthesized beam which then decreases the computation time.

In Table 3 we also show the parameters for the HTRU survey performed recently with the 13-beam Multibeam receiver on the Parkes radio telescope at 1.4 GHz (Keith et al. 2010). This is the most recent and relevant large area survey of the southern sky performed at high latitudes (from the Galactic plane up to $b = \pm 15^\circ$). In what follows, we adopt the HTRU mid-latitude survey as a reference to check the consistency of our results with previous surveys.

In Table 3 we also quote other relevant parameters for the present analysis, as, for example, the adopted per pointing observation dwell times, along with the corresponding total time needed to cover a 108 deg^2 area of sky. We here assume that beams are non-overlapping. These effects need to be taken into account when setting up an actual observation strategy, and will increase the required observation time for a given field by a factor of less than two.

4. RESULTS FOR LARGE AREA SEARCHES

In this section, we will first discuss prospects for current and future radio telescopes to detect bulge MSPs in large area surveys (meaning several square degrees of sky), and then quantify the number of MSP detections that would be required to unambiguously confirm the existence of a bulge population in addition to the observed thick-disk population of MSPs.

4.1. General Reach of Current and Future Radio Surveys

For each simulated MSP in the bulge, modeled according to Section 2, we compute the corresponding 10σ detection sensitivity flux, following Equations (5) and (6) for the observation scenarios in Table 3. In Figure 6 (top panel) we show the distribution of all bulge MSPs in the flux density (at 1.4 GHz) versus period plane. As mentioned above, the adopted period distribution (Lorimer et al. 2015) has a mean of 5.3 ms. We note that this value is slightly higher than what is typically adopted as a mean MSP period, $P \sim 3$ ms.

Assuming a lower mean spin period would somewhat reduce our estimates since finding fast-spinners is harder due to scattering and Doppler smearing in binaries. However, since the threshold sensitivities in the top panel of Figure 6 depend only mildly on the spin period, we do not expect a large effect.

We simulate sources with a period between 0.4 and 40 ms. The corresponding radio fluxes at 1.4 GHz span from about 10^{-5} mJy up to about 0.9 mJy (we note that the lower flux limit is a consequence of the adopted luminosity function and observationally neither relevant nor well constrained). However, not all the sources with high flux densities can be detected for our three reference scenarios. Colored dots show which of the sources would be detected by our assumed measurements with GBT, MeerKAT, and SKA-mid with 10σ significance. The GBT will be able to detect sources down to about 0.03 mJy and periods in the range of $1 \text{ ms} \leq P \leq 40 \text{ ms}$. MeerKAT and SKA-mid, instead, will probe radio fluxes as low as 0.03 mJy and 0.01 mJy, respectively, in the full period range of the population above 0.8 ms. We also overlay the sensitivity of the currently most sensitive survey covering the relevant sky area, the Parkes HTRU mid-latitude survey (assuming $\text{DM} = 300 \text{ pc cm}^{-3}$). No source lies above this line, showing that such a survey is not quite yet sensitive enough to detect the bulge MSPs, however it is evident that it starts to scratch the high-luminosity tail of this population. On the other hand, it is clear that there will be a progressive improvement in the number of sources detectable by the three telescopes we consider. With GBT the gain in sensitivity would already result in hundreds of sources being above threshold with only 20 minutes integration time per sky position (although the total time to survey a large enough region of the sky still remains very large, as we will see below).

The bottom panel of Figure 6 clarifies what is the distribution of DM for the simulated bulge population and the corresponding scattering time, τ_{scatt} . Most of the sources have DM in the range 100–800 pc cm^{-3} . The sharp and dense features at around 800 and 1800 pc cm^{-3} correspond to regions very close to the Galactic center and are due to discrete “clumps” of enhanced free electron density that are included in the NE2001 model (see Tables 5–7 in Cordes & Lazio 2002; these are also visible in Figure 5). The scattering times follow the trend of the adopted reference model from Bhat et al.

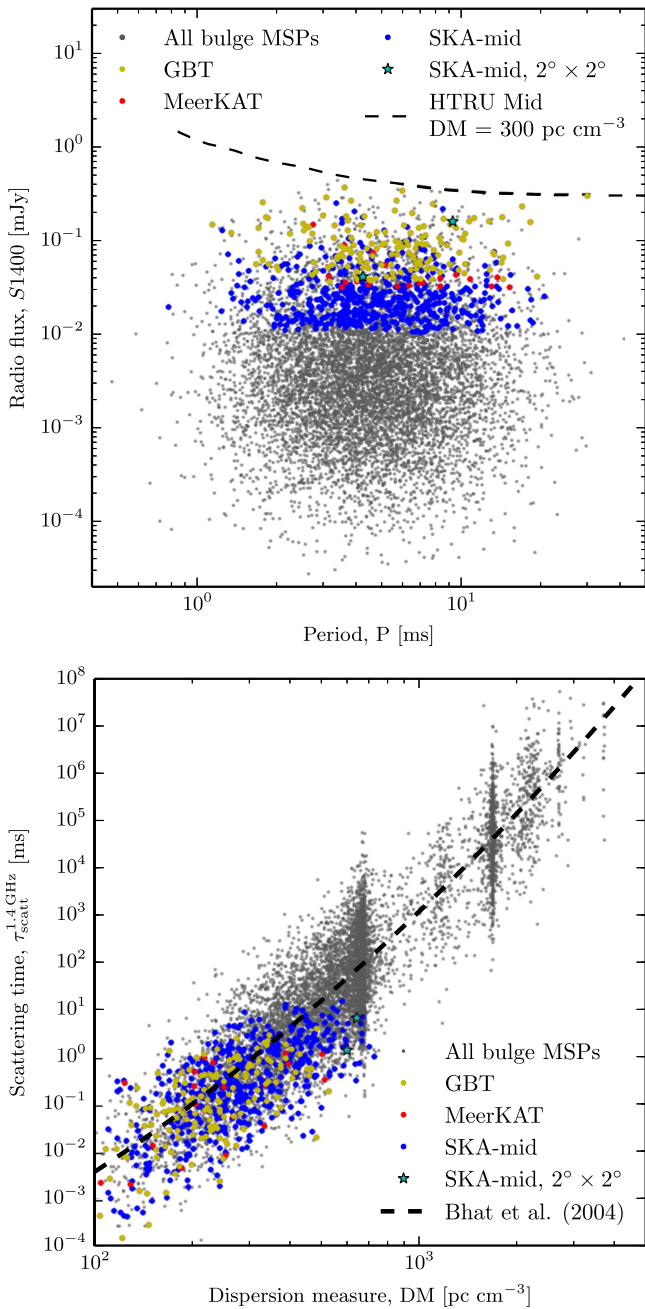


Figure 6. We show the simulated bulge population of MSPs, modeled from gamma-ray observations as described in the text, both in the period vs. flux density plane (*top panel*), and in the dispersion measure vs. scattering time plane (*bottom panel*). Gray dots denote the entire MSP bulge population. The colored dots show which of these sources would be detectable with the various observational scenarios that are described in Table 3. Namely, yellow points correspond to sources that will be detectable by GBT, MeerKAT, and SKA-mid, red points for sources detectable by MeerKAT and SKA-mid, and blue points for sources detectable only by SKA-mid. The dashed black line in the upper panel corresponds to the minimum flux sensitivity of the Parkes HTRU mid-latitude survey at a reference value of $DM = 300 \text{ pc cm}^{-3}$, and rescaled for the 10% duty cycle we adopt in the present work. In the bottom panel we show also the average relation from Bhat et al. (2004) as dashed black line. The visible structures correspond to specific sky regions with very large DM, see Figure 5.

(2004) as expected, with a significant scatter. In general, scattering times larger than 5–10 ms prevent the sources from being detected, and the limiting factor in Equation (6) is indeed τ_{scatt} . For scattering times smaller than 5–10 ms, instead, a

source might be detected or not depending on its spin period. The GBT and MeerKAT can detect most sources with DM up to 550 pc cm^{-3} , while none with $DM \sim 600\text{--}800 \text{ pc cm}^{-3}$. On the other hand, SKA-mid will be able to detect MSPs that suffer from larger scattering, up to about 800 pc cm^{-3} . In particular, we can see that with SKA-mid we will be able to detect a few sources with high DM ($\sim 600\text{--}800 \text{ pc cm}^{-3}$) and in the few inner degrees of the Galactic center, namely the inner $2^\circ \times 2^\circ$ degrees. In general, SKA can probe more sources because of the higher sensitivity. Since the luminosities are uncorrelated with spin period and other parameters, it can pick out the sources that have high DM, but luckily have anomalously low scattering. Moreover, the central observing frequency of SKA (assumed here) is 1.67 GHz, which is slightly higher than GBT and MeerKAT. Given the strong frequency dependence of the scattering time, it reduces temporal scattering by a factor of around two.

4.2. Optimal Target Regions

We now investigate what the detection prospects are for large-area surveys performed with the three instrumental reference scenarios (namely with GBT, MeerKAT, and SKA-mid configurations). For each instrument we show, in the top panels of Figures 7–9, the number of bulge MSPs that can be detected with 10σ significance and the corresponding number of detectable disk MSPs in parenthesis (as modeled in Section 2). We analyze a region in the inner Galaxy defined by $|\ell| < 9^\circ$ and $|b| < 9^\circ$, and we split it in squared subregions of size $2^\circ \times 2^\circ$. Integration times per pointing and central observing frequencies are as shown in Table 3.

An alternative way to visualize the prospects for detection of the bulge population above the disk population is to plot in the x - z plane the sources detectable along the lines of sight toward the inner Galaxy. Emphasizing sources detectable from these directions helps in understanding (a) what the contamination is from foreground disk sources, and (b) how deep toward the Galactic center we can probe the bulge population. In the bottom panels of Figures 7–9 we show the spatial distribution of the simulated bulge and disk MSPs in the x - z plane and we highlight the sources that can be detected in the region $|\ell| < 2^\circ$ and $|b| < 20^\circ$ (which corresponds to the inner Galaxy region analyzed by Calore et al. 2015b).

In Figures 7–9 we show the number of detectable sources with GBT, MeerKAT, and SKA-mid, respectively, for 20 minutes observation dwell time per pointing. For the GBT scenario the number of detectable bulge MSPs is always lower than two for each sky subregion and, depending on the subregion, the number of detectable disk MSPs is comparable. On the other hand, in the case of MeerKAT and even more for SKA-mid, there is an optimal search region, which is a few degrees south of the Galactic center, at approximately $|\ell| \leq 1^\circ$ and $-5^\circ \leq b \leq -3^\circ$, where the number of detectable bulge MSPs is the largest. While for MeerKAT the number of bulge MSPs in such an optimal spot is still comparable with the number of foreground thick-disk MSPs, in the case of SKA-mid (for which the optimal target region slightly shifts toward lower latitudes, $|\ell| \leq 1^\circ$ and $-3^\circ \leq b \leq -1^\circ$) the number of detectable bulge sources is as high as 12 per 4 deg² and the corresponding detectable disk MSPs are always about half of the number of bulge MSPs detectable in the same subregion.

Typically, the suppression of the number of detectable sources along the Galactic disk comes from strong scattering

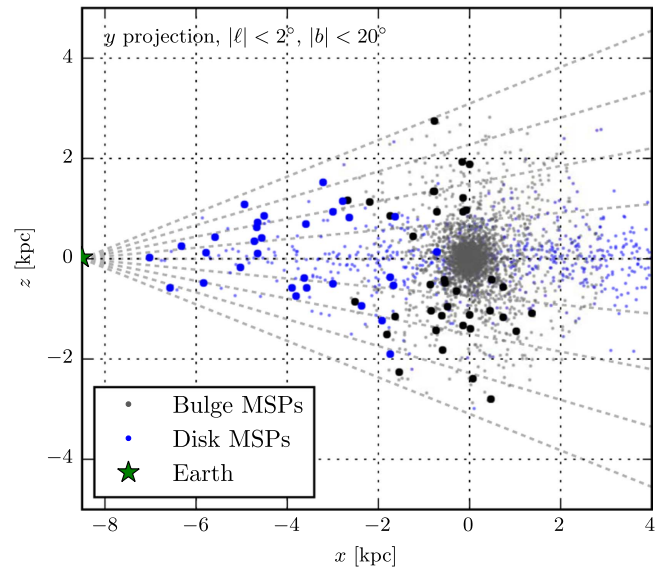
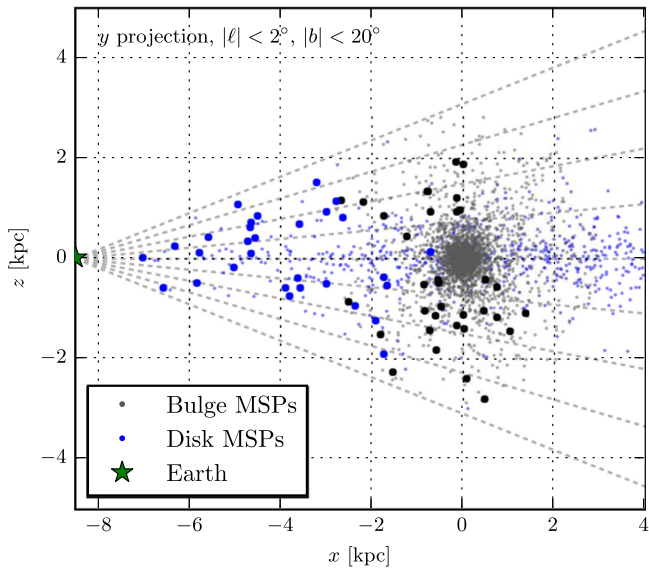
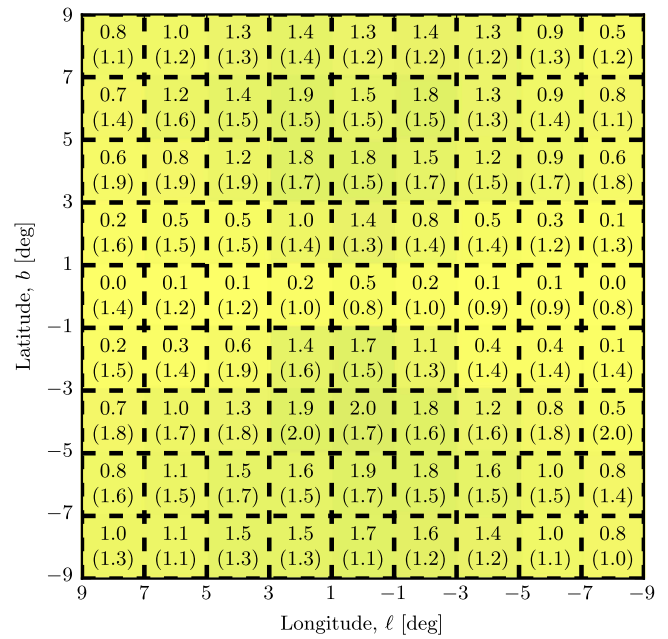
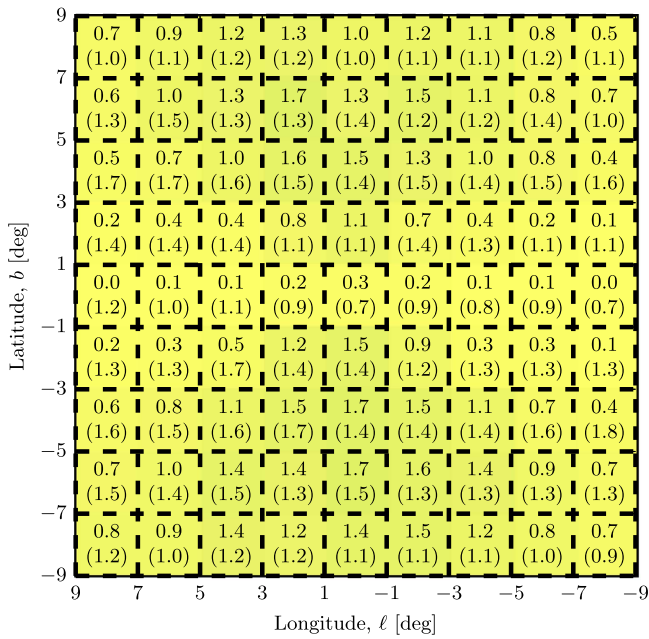


Figure 7. *Top panel:* GBT detected sources from bulge (disk) population for 20 minutes integration time per pointing (250 h for each field of $2^\circ \times 2^\circ$) at 1.4 GHz. The number of sources detectable is also represented by the colored background. *Bottom panel:* x - z projection of simulated bulge (*thin black dots*) and disk (*thin blue dots*) MSPs. *Thick black dots* refer to bulge MSPs detectable toward the inner Galaxy, $|\ell| < 2^\circ$ and $|b| < 20^\circ$, with the GBT survey. *Thick blue dots* are instead the disk MSPs that would be detected by the survey in the same region of interest.

Figure 8. Same as Figure 7, but for a MeerKAT-like survey with parameters as described in Table 3.

effects discussed in Section 3. We will discuss the advantage (against scattering effects) of using higher frequency surveys in Section 6. While from the bottom panels of Figures 7 and 8 it is evident that, for the GBT, the bulge MSPs that lie truly at the Galactic center and along the Galactic disk remain hard to identify for those two scenarios, the predictions improve with SKA-mid. From the bottom panel of Figure 9, indeed, we can see how the detectability of bulge MSPs from the very central region of the bulge is less affected by pulse broadening and the contamination along directions toward the inner Galaxy is lower. Interestingly, SKA-mid will be able to probe sources residing in the innermost degree, $|\ell| \leq 1^\circ$ and $|b| \leq 1^\circ$ (those

same sources are the ones highlighted in Figure 6; note that Figure 9 shows average values). These sources happen to have a very low scattering broadening, which is, in our case, possible even in the inner Galaxy, since we adopt a large variance in the scattering time of individual sources. The bottom panel of Figure 9 clearly demonstrates the detection power of SKA-mid. While the number of detectable thick-disk MSPs remains limited to a few objects (simply because the density of thick-disk sources is relatively small), the number of bulge MSPs that can be observed is very large.

For GBT, observations of sky areas as large as 4 deg^2 are mainly limited by the small size of the telescope beam at high frequencies and to cover a $2^\circ \times 2^\circ$ region of sky with the GBT at 1.4 GHz, a total observation time of about 83 hr is required. This makes the survey of larger areas unfeasible, and in any case it would lead to a maximum of two detections per 4 deg^2 . The much larger field of view of MeerKAT, with respect to the

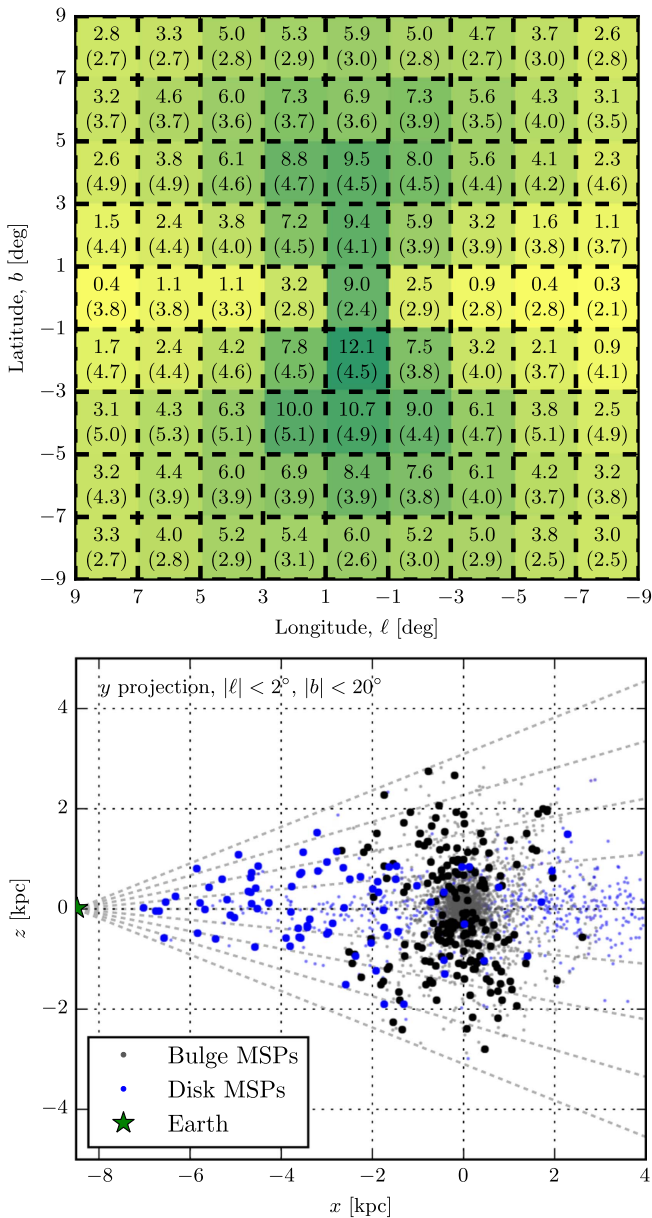


Figure 9. Same as Figure 7, but for an SKA-mid-like survey with parameters as described in Table 3. Here, one can nicely see a dearth of detectable MSPs in the shadow of the Galactic center as well as in front of the Galactic center. In both cases, this is presumably due to the scattering and uncorrected dispersive smearing.

GBT beam size, allows for surveying the same 4 deg^2 area in a much shorter time, i.e. about 2.5 hr. Analogously, for SKA-mid, about 3.5 hr are required to survey the region. This might enable ~ 100 hr long surveys that can scan sky areas about 40 times larger than our 4 deg^2 subregion and thus probe ~ 100 bulge MSPs (in the most promising sky regions).

As mentioned above, limiting factors, like a reduced maximum baseline and limited computation power, will likely increase the required observation times by a factor of two or more.

To understand the interplay among area surveyed the total integration time and predicted number of detectable bulge MSPs (and foreground thick-disk MSPs) in Table 3, we quote the number of bulge and foreground thick-disk MSPs that would be detectable by the GBT, MeerKAT, and SKA-mid for

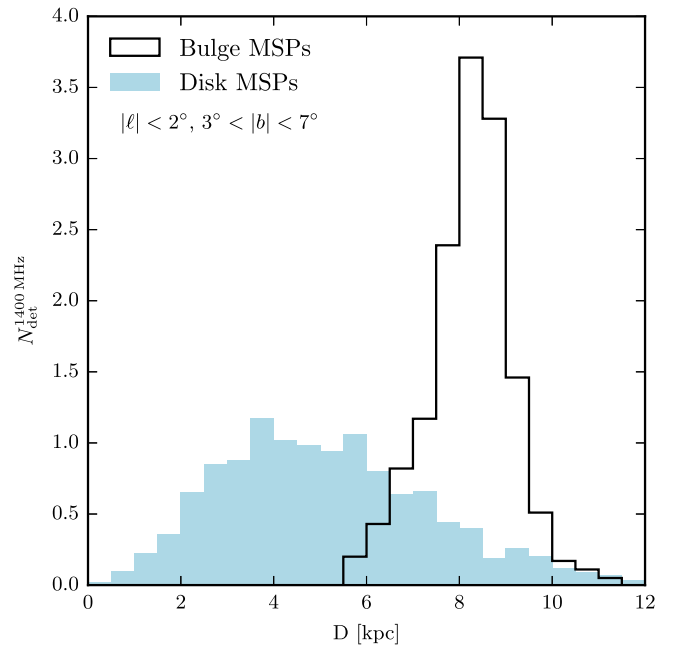


Figure 10. Histogram of distances of detected bulge (black) and disk MSPs (blue), assuming the MeerKAT reference survey in Table 3. Bulge and disk components can be clearly separated. The bulge component should appear as a clear excess of sources with dispersion measures that indicate distances around 8.5 kpc.

a large-area survey of 108 deg^2 and 20 minutes of dwell time per pointing. The chosen large-area survey is defined by the 27 4 deg^2 sky areas that have a large yield of detectable sources (larger than six) for the SKA-mid scenario. This region corresponds to $(|l| < 5^\circ \text{ and } 3^\circ < |b| < 7^\circ)$, plus $(|l| < 3^\circ \text{ and } 1^\circ < |b| < 3^\circ)$, plus $(|l|, |b| < 1^\circ)$. It is evident that GBT and MeerKAT might lead to comparable numbers of detected MSPs from the bulge (~ 30 – 40 sources). Analogously, for both observational scenarios the number of detectable thick-disk MSPs is comparable to the bulge ones, and thus this is not really a promising strategy given the strong contamination from disk sources. Moreover, the time needed for GBT to survey a 108 deg^2 area is about 30 times larger than the total time required for the same survey with MeerKAT. In this respect, large-area surveys will not be feasible with the GBT but might be promising with MeerKAT. SKA-mid clearly improves those predictions; it allows a discrimination between bulge and thick-disk MSPs in a reasonable total integration time (92 hr). A large-area survey with time per pointing of about 20 minutes can thus be an optimal strategy for SKA-mid to identify bulge MSPs.

In conclusion, prospects for large-area surveys are extremely good for upcoming radio telescopes, albeit they are less promising for current observations through the GBT. With GBT, the main limitations are represented by the very large integration time required to survey a small sky area and the relatively low number of detectable bulge and disk sources, which would make it harder to disentangle the two populations. On the other hand, with MeerKAT, and later with SKA-mid, the smaller required total integration time together with the higher sensitivity will allow to quickly probe large areas and detect a very significant fraction of the MSP bulge population.

4.3. Discrimination of Bulge and Thick-disk Populations

In Figure 10 we show a histogram of the distances of all MSPs that would be detected by our MeerKAT reference survey in eight 4 deg^2 subregions below and above the Galactic center, $|\ell| < 2^\circ$ and $3^\circ < |b| < 7^\circ$. The adopted survey region is exemplary, and chosen because it provides a good MSP yield (see Figure 8) while at the same time having a relatively low contamination with foreground sources. Furthermore, we concentrate on MeerKAT to obtain conservative estimates. The deeper observations with SKA would only increase the relative number of bulge sources, and simplify a discrimination from foreground MSPs. For the adopted survey and target region the number of detected bulge sources would be 14.3. The number of detected disk sources in our reference scenario would be 12.2. It is already clear that the distance distributions are very different, with the thick-disk distribution peaking very broadly at 4 kpc, whereas the bulge population has a pronounced peak around 8.5 kpc.

In order to provide a first estimate for the *minimum* number of bulge MSPs that need to be detected in order to identify the bulge population with a statistical significance of 99.7% confidence level (CL) above the foreground of thick-disk MSPs, we perform a simple statistical test as follows. Let μ_i^{disk} and μ_i^{bulge} be the expectation values for the disk and bulge components, respectively, as shown in Figure 10 (i refers to individual distance bins). We consider the ‘‘Asimov data set’’ (Cowan et al. 2011) $c_i^A = \zeta(\mu_i^{\text{bulge}} + \mu_i^{\text{disk}})$, where c_i^A denotes the number of measured MSPs in a certain distance bin, and ζ is a rescaling factor with respect to the number of sources shown in Figure 10. It accounts for the effect of surveying a smaller region of the sky. We calculate the Poisson likelihood both for the null hypothesis $\mu_i^{\text{null}} = \zeta\mu_i^{\text{disk}}$ and the alternative hypothesis $\mu_i^{\text{alt}} = \zeta(\mu_i^{\text{bulge}} + \mu_i^{\text{disk}})$. We numerically solve for ζ by requiring that the minus-two log-likelihood ratio $-2 \ln(\mathcal{L}_{\text{null}}/\mathcal{L}_{\text{alt}})$ equals nine. The value that we find is $\zeta = 0.24$, which corresponds to the detection of 2.9 disk and 3.4 bulge sources. Note that we implicitly assume here that the normalization of the disk component can be constrained from other regions of the sky (since we keep ζ fixed when calculating $\mathcal{L}_{\text{null}}$). Indeed, the main reason for the low number of only 3.4 required bulge detections is the low background from the disk at distances around ~ 8.5 kpc distance.

We conclude that the detection of a handful of bulge sources is enough, provided that their distances can be estimated accurately enough, to start discriminating the bulge and disk components in a statistically meaningful way. The NE2001 model provides DM-based distance predictions, typically with 25% fractional uncertainty. This will be useful for associating MSP discoveries with a bulge population. Parallax distance measurements (or lower limits) using very-long-baseline radio interferometry (VLBI) could also be used, but, for the weakest sources, the sensitivity of current VLBI arrays may be insufficient for detection. However, we stress that a robust statistical statement should ideally be based on a physical model for the bulge distribution (which might not necessarily include sources in the inner kpc) and be marginalized appropriately over disk and bulge profile uncertainties, the total number of disk and bulge sources, and include uncertainties in the DM-based distance measure. However, our above estimates suggest that a robust detection of the bulge MSP component should be possible once the radio pulsation from the first couple of bulge sources has been observed.

5. RESULTS FOR TARGETED SEARCHES

Deep searches for radio pulsations toward unassociated *Fermi* gamma-ray sources have been extremely successful in discovering new MSPs (Ray et al. 2012; Abdo et al. 2013; Grenier & Harding 2015). This is mostly due to the fact that targeted searches allow for deeper observations than time-intensive large area surveys. It is thus natural to assume that the same strategy should also be useful for identifying the bulge population of MSPs. Interesting targets in this case are unassociated *Fermi* sources in the inner Galaxy, but also potential sources that remained below the *Fermi* source detection threshold could be valuable targets. Candidates for the latter were recently identified as wavelet peaks in the analysis of Bartels et al. (2015) and as hotspots in the analysis of Lee et al. (2015). We will from here on refer to all of these potential sources as *MSP candidates*, and discuss the prospects for identifying their radio pulsation signal.

In contrast to the above discussion about large area surveys, the prospects for radio targeted searches depend strongly on the details of gamma-ray and radio beaming. The reason is that the success of deep, targeted, follow-up radio searches hinge on whether gamma-ray bright sources are also bright in radio. Although even a strong gamma-ray/radio correlation would leave our above discussion about prospects for large area surveys completely untouched, it would be very beneficial for targeted searches.

Obviously, not every MSP candidate found in *Fermi* data will correspond to an MSP. The odds for this depend on the density of MSPs and other sources in the inner Galaxy, the statistical significance of the MSP candidate, its spectrum, and its variability. However, we will focus here on the radio detection sensitivity and the effect of a possible gamma-ray/radio correlation. To this end, we will simply assume that all of our MSP candidates correspond, in fact, to MSPs, and that their localization is known with much better accuracy than the beam size of theGBT.

As an instructive example, we will here use the 13 unassociated 3FGL (Acero et al. 2015) sources that were identified as MSP candidates in Bartels et al. (2015) based on their spectrum and the absence of variability. We stress that *this does not mean that these sources are necessarily the best targets for follow-up searches*. However, their gamma-ray brightness, as well as their positions in the inner Galaxy, have typical values that should be comparable in *any* list of follow-up targets. Studying the radio sensitivity for targeted observations at the position of these sources is hence indicative for targeted observations of any sources related to the *Fermi* GeV excess.

5.1. On the Gamma-Ray Radio Correlation

As a very rough estimate, only bulge MSPs with a luminosity of at least $L_\gamma \gtrsim 10^{34} \text{ erg s}^{-1}$ will show up as MSP candidates in *Fermi*-LAT gamma-ray observations (potentially with very low significance). The required luminosities for detection are typically higher (see Abdo et al. 2013; Petrovic et al. 2014b; Bartels et al. 2015), but the exact value does not matter for the following discussion. We will show that for such gamma-ray bright MSPs, the radio emission is also very well above the average, and exploit it when predicting prospects for radio follow-up observations.

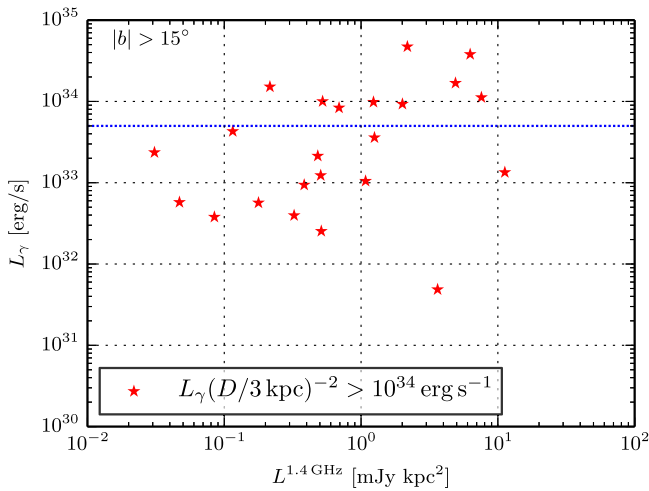


Figure 11. Gamma-ray luminosity vs. radio pseudo-luminosity at 1.4 GHz, for high-latitude ($|b| > 15^\circ$) MSPs from Abdo et al. (2013) that pass the flux threshold as defined in the figure. We also show the gamma-ray luminosity threshold ($L_\gamma > 5 \times 10^{33} \text{ erg s}^{-1}$) that we use for selecting radio luminosities for luminous gamma-ray MSPs (see text for details).

We emphasize that the adopted estimate depends critically on possible selection effects. In almost all cases, *Fermi* sources were identified as MSPs by the observation of radio pulsation. This will, in general, bias a relation that is just based on radio-observed MSPs, since radio-quiet MSPs would be listed as unassociated *Fermi* sources. Below, we will conservatively take this effect into account by assuming that all unassociated non-variable high-latitude sources are radio-quiet MSPs.

Roughly 1/3 of the MSPs discovered in *Fermi* targeted searches have been shown to be in eclipsing “black widow” or “redback” systems (Ray et al. 2012). While eclipses can lead to MSPs being missed in a survey, we conservatively estimate that this is about a 15% reduction in the potential yield of a wide-field survey—assuming that 30% of the sources are eclipsed 50% of the time. In the following discussion we will study the gamma-ray and radio emission properties of MSPs and unassociated sources based on the sources listed in the Second Pulsar Catalog, 2PC (Abdo et al. 2013), and in the 3FGL (Acero et al. 2015). In order to select bright gamma-ray sources we adopt a *flux* threshold that corresponds to $L_\gamma = 10^{34} \text{ erg s}^{-1}$ at 3 kpc distance. This trivially includes all luminous (namely $L_\gamma > 10^{34} \text{ erg s}^{-1}$) MSPs within 3 kpc distance from the Sun, but also all unassociated sources that could be luminous MSPs in that volume. As a *spatial* cut, we adopt $|b| > 15^\circ$, which practically removes all young pulsars and other disk sources and leaves only high-latitude sources (predominantly active galactic nuclei).

In Figure 11 we show the gamma-ray luminosity and the radio pseudo-luminosity of high-latitude *Fermi* MSPs from the 2PC (Abdo et al. 2013). In addition, we also include the MSPs PSR J1816+4510, PSR J1311–3430, PSR J0610–2100, PSR J1903–7051, and PSR J1745+1017, for which we take the gamma-ray fluxes from the 3FGL, and radio fluxes and distance measures from Barr et al. (2013), Camilo et al. (2015), Pallanca et al. (2012), Ray et al. (2013), Stovall et al. (2014). Almost all sources with $L_\gamma \geq 5 \times 10^{33} \text{ erg s}^{-1}$ have radio luminosities above around 0.5 mJy kpc². This is *above* the median of our reference radio luminosity function (0.3 mJy kpc²). Somewhat contrary to the conventional

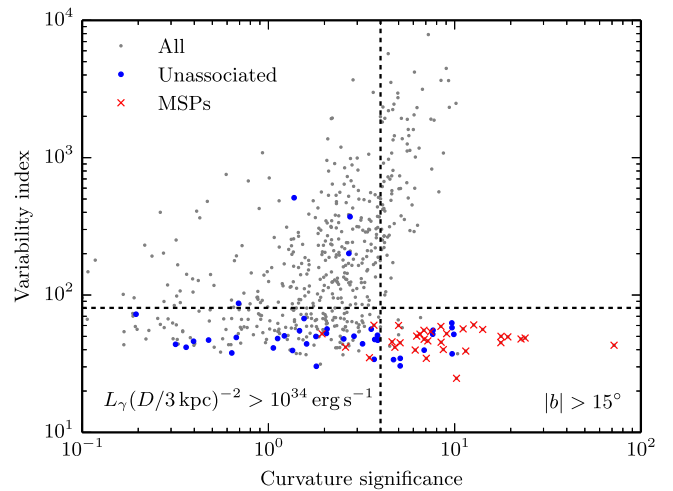


Figure 12. Curvature significance vs. variability index, for *all* high-latitude sources that pass the flux threshold as indicated in the text and in the figure. We furthermore indicate unassociated sources and MSPs. The horizontal line separates variable from non-variable sources, the vertical line separates sources with a significantly curved spectrum from those whose spectra are power-law like. The full source list and definitions can be found in Acero et al. (2015).

wisdom that gamma-ray and radio luminosities are truly uncorrelated, this does suggest a loose correlation between these quantities.¹⁶ However, given the low number of sources, little can be said about the nature of the correlation (e.g., whether it is linear in log–log space, or whether it continues to lower luminosities). We will for now take this observation at face value, and comment below in Section 6 on how the results might change when any correlation is neglected.

In order to estimate how many MSPs that are in bright gamma-rays could have remained undetected in radio, we show in Figure 12 high-latitude MSPs, unassociated and other sources from the 3FGL, as a function of the variability index and the curvature significance (for definitions see Acero et al. 2015). We only show sources that pass the flux threshold that we discussed above.¹⁷ These parameters provide useful discriminators, and help to separate pulsar-like sources from other sources at high latitudes, such as active galactic nuclei. One can clearly see that MSPs consistently have a low variability index (values below around 80 indicate non-variable sources), and most of them feature a curved spectrum that leads to a large curvature significance. Many of the unassociated sources appear to be non-variable as well, and a few of them feature high curvature significances. On the other hand, most of the remaining bright high-latitude sources are variable, since the dominant fraction of the extragalactic sources is formed by (variable) active galactic nuclei.

If we focus on the indicated region in Figure 12 with non-variable sources and high curvature significance (lower-right corner), it is clear that there is only a little room for bright gamma-ray MSPs to “hide” as unassociated sources. The number of MSPs in that region could be at most a fraction $\sim 30\%$ larger with respect to what is already known. These additional MSPs, which would not yet have shown up in radio

¹⁶ A simple estimate for the p -value for this happening by chance can be obtained as $p \sim 0.5^8 \approx 0.004$, given that we have seven sources, which corresponds to 2.8σ .

¹⁷ Note that Figure 12 shows 31 MSPs, and Figure 11 shows 23. The 8 MSPs that are missing in Figure 11 are either without radio detection (in two cases) or the detected flux is not yet published.

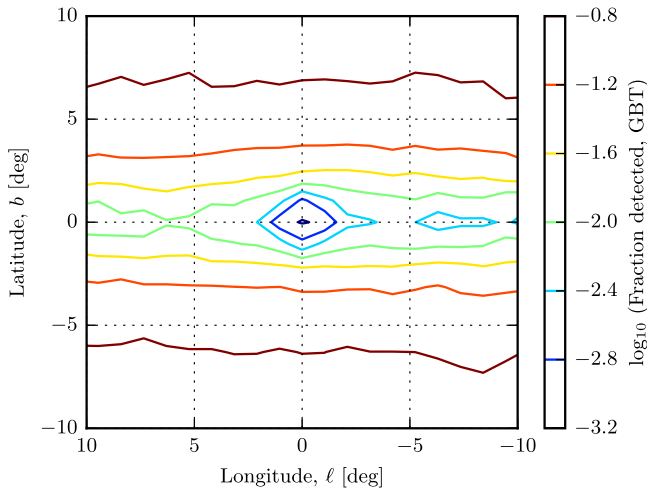


Figure 13. Fraction of gamma-ray bright bulge MSPs along the line of sight that can be detected with the GBT survey from Table 3. See text for details of the empirically derived radio luminosity of the MSP population.

searches, could potentially be radio quiet, and weaken the above loose gamma-ray/radio correlation.

In order to model the radio luminosity of MSP candidates from *Fermi* observations in a way that is motivated by actual radio observations, we adopt the following simple strategy. In 60% of the cases, we will draw a random radio luminosity from the nine MSPs in Figure 11 with a gamma-ray luminosity $L_\gamma > 5 \times 10^{33} \text{ erg s}^{-1}$, since only such bright sources would appear as MSP candidates associated with the bulge population. In the other 40% of the cases we will assume that radio luminosity is zero, to account for fact that some or most of the unassociated sources could be actually radio-dim MSPs, and for the fact that that some of the MSPs in Figure 12 are either radio-quiet or have no published fluxes. This procedure is somewhat ad hoc, but is completely data driven and should give a reasonably accurate description of the detection prospects of MSP candidates. However, the uncertainties associated with this method are certainly large, and likely affect the resulting detection probability by a factor of roughly two (which we estimate from the typical Poisson error associated with drawing from just nine sources).

5.2. Detectability

In Figure 13, we show the detection probability of gamma-ray bright bulge MSPs in different regions of the inner Galaxy, assuming that each source is observed by the GBT as summarized in Table 3. We note that here we adopt integration time per pointing of 60 minutes for all three observational scenarios (see below). We adopt the empirically derived radio luminosity function for gamma-ray bright MSPs as discussed above, and calculate the probability that a bulge MSP along the line of sight can be detected, weighted by the source density in the bulge and the volume factor.

At high latitudes the probability is nearly 10%, whereas close to the Galactic disk it is well below 0.1%. This already indicates that follow-up observations of individual MSP candidates are rather challenging, even if their position is known precisely. This is true in particular close to the Galactic disk.

In order to get an estimate for the detection probability of a typical bulge MSP candidate, we average the detection

Table 4

Projected Number of Detections for Follow-Up Radio Searches in 20 MSP Candidates, Assuming that All of the MSP Candidates are Indeed Gamma-Ray Luminous MSPs in the Bulge Region

Instrument	t_{obs} total	Detection of MSP candidates	
		Probability	Number (20 total)
GBT	20 h	18.4%	3.7
MeerKAT	20 h	20.5%	4.1
SKA-mid	20 h	40.8%	8.2

Note. Radio luminosity of gamma-ray luminous MSPs is estimate from a flux-limited sample of high-latitude MSPs and unassociated sources. Although the results were obtained in an observation-driven approach, they are uncertain by at least a factor of two and of indicative value only. Caveats are discussed in the text.

probability over the 13 reference 3FGL sources from Bartels et al. (2015). The resulting probabilities are summarized in Table 4 for the different observational scenarios from Table 3. We find average probabilities of 18% in the case of GBT, which grow to 40% in the case of SKA-mid.

Our results indicate that, on a short timescale, radio follow-up observations of MSP candidates with the GBT or similar instruments are the most promising strategy to actually find the first MSPs from the bulge region. The numbers in Table 4 are very promising. However, as mentioned above, additional effects need to be taken into account that will further reduce the detection probabilities. First, not every MSP candidate will correspond to an MSP. This will reduce the number of possible detections by the likelihood for a given MSP candidate to correspond to an MSP (probably by up to a factor of two, see Bartels et al. 2015). Second, source localization is critical. The GBT beam size of 0.14 deg FWHM is comparable to the localization accuracy that can be reached with *Fermi* at 68% CL. Hence, several pointings might be necessary to fully cover the area in which the radio emission from an MSP candidate could lie. Both of the caveats need to be carefully taken into consideration when planning actual observations. Furthermore, we note that targeted searches using long, 60 minutes integration times have the additional issue that MSPs often reside in binary systems and Doppler smearing of the pulsed signal is difficult to correct in a blind search if the integration time is a significant fraction of the orbital period. This is further discussed in Section 6.

Finally, in Figure 14 we show the number of sources that will be detectable with increasing GBT targeted observations for a fixed total integration time. In general, it is more promising to use a shorter dwell time and allow more pointings. While with a total integration time of 10 hr for only a few source, out of 30 pointings can be detected, a total integration time of 100 hr distributed over 30 spots, in the sky would enable the detection of about 8 sources.

6. DISCUSSION

The predicted radio emission of the MSP bulge population has to be consistent with the results of existing pulsar radio surveys. Here we will concentrate on the consistency with the Parkes HTRU mid-latitude survey, which covers latitudes in the range $3.5 < |b| < 15^\circ$, and hence regions of the sky that we find to be the most promising for finding MSP bulge sources (at lower latitudes scattering becomes increasingly

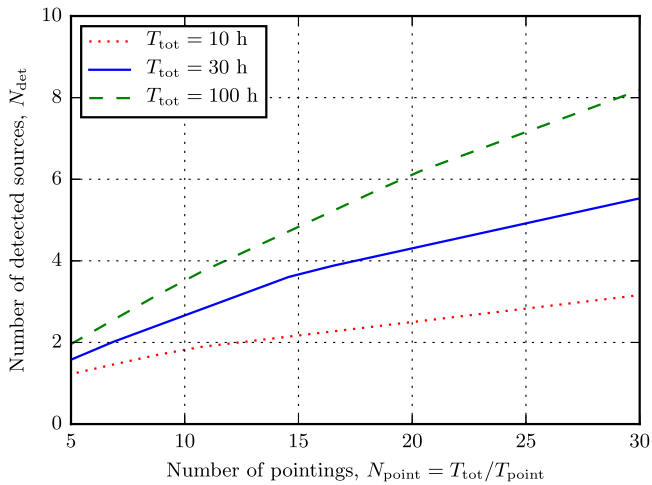


Figure 14. Number of detectable sources as a function of the number of targeted observations using GBT with total integration time of 10 hr (dotted red), 30 hr (solid blue), and 100 hr (dashed green).

important). We find that, with the configuration listed in Table 3, the HTRU mid-latitude survey should have detected around seven MSPs from our reference bulge population and luminosity function (“Model 3”). For the alternative luminosity functions Model 1 (2) we find that 10 (4) bulge MSPs should have been seen.

Interestingly, the HTRU mid-latitude survey has detected only one field MSP within 3 kpc of the Galactic center, J1755–3716 at 6.38 kpc distance (Ng et al. 2014). This source could be just on the edge of the bulge population. This is, on first sight, slightly inconsistent with the number of bulge MSPs that Parkes should have seen according to our above estimates. For reasons that we discuss next, we do not consider this discrepancy as severe, given that the HTRU sensitivity is just scratching the brightest of the bulge MSP sources. However, it is an indication that the bulge MSPs are, in principle, in reach of current instruments.

There are a number of possible interpretations for the apparent non-observation of a few bulge MSPs with Parkes HTRU. The first possibility is that the bulge MSP population has different properties than derived in this work, since it e.g., does not fully account for the observed gamma-ray excess in the inner Galaxy. This is certainly a possibility, but the inconsistency between Parkes HTRU predicted and actual detected sources is not strong enough to make definitive statements here (this would likely change if future surveys do not find bulge MSPs either). Another concern might be that we overestimate the sensitivity of the Parkes HTRU. This seems unlikely as our faintest simulated sources detected with Parkes HTRU (mid-latitude) have fluxes around 0.18 mJy, which is compatible with the faintest measured MSPs with Parkes (Levin et al. 2013). However, given that estimates of detection thresholds are very sensitive to a large number of parameters, we cannot exclude this possibility.

It could be that the radio luminosity function of bulge MSPs is significantly different from what is observed in globular clusters. Given the possibly different formation histories of MSPs in globular clusters and the bulge, this cannot be excluded. Lastly, it could be that a number of bulge sources were already discovered by the Parkes HTRU, but the DM-based distance measure is biased to lower values such that the MSPs appear closer and less luminous than they actually are.

We emphasize that most of the above caveats related to the sensitivity of the Parkes HTRU do not directly apply to the other reference surveys from Table 3. Already, observations with the GBT will probe significantly fainter sources, which reduces the dependence on the details of the radio luminosity function in the bright tail. Indeed, we find that the number of sources detectable by the GBT for Model (1, 2, 3) is (162, 127, 151), and hence varies by less than 15% (see Table 2) from our reference result. However, a possible bias of DM-based distance measures cannot be excluded and would also affect results by the GBT and other instruments.

About three quarters of all field MSPs are bound in *binary systems*, with orbital periods ranging from 94 minutes to hundreds of days (Stovall et al. 2013, 2014). Given the many free orbital parameters, the induced Doppler shift in the observed pulse period can make an identification of the pulsation extremely difficult because it smears out the periodic signal in the Fourier domain. Using acceleration search techniques (e.g., Ransom 2001), it is possible to compensate for orbital motion; however, such techniques are only sensitive in cases where the observing dwell time is less than about a tenth of the orbital period. As such, this imposes a practical limitation to the beneficial dwell time per sky pointing.

Although the observation time per pointing in our described targeted searches are comparable to the smallest observed orbital period, which would cause problems for our reference searches, most other observed orbital periods are much larger, and we do not expect a very strong effect on our results. As we discussed above, orbits that are at least ten times longer than the dwell time per survey pointing should be enough.

It is conventionally assumed that gamma-ray and radio luminosities are uncorrelated. However, we showed that high-latitude gamma-ray MSPs and unassociated *Fermi* sources suggest a loose gamma-ray/radio correlation. We used this relation when estimating the radio detection probabilities for bright gamma-ray MSPs in the bulge. If we would neglect this correlation, and assume instead that a given MSP candidate source has a radio luminosity that is randomly drawn from our reference luminosity function “Model 3,” the detection prospects in the case of e.g., GBT in Table 4 would reduce from ~18% to <10%. Hence, the presence or absence of a gamma-ray/radio correlation has a significant impact on the prospects for radio follow-up searches for MSP candidates. In this context, we emphasize that if there are only a few dozen MSP candidates, then searching each one for 1 hr or more would still take much less time than blindly searching the dozens of square degrees of sky needed to potentially lead to the same number of MSP detections.

From Figure 6 it is clear that the main limitation to the detection is scattering. In principle, this can be mitigated by observing higher frequencies, since the scattering time roughly scales with $\nu^{-4.4}$. However, the price for this lower scattering time is a reduced signal flux because of the steep source spectrum. We use $\alpha_\nu = 1.7$ as the spectral index to rescale the flux density from one frequency to another, with flux density $S_\nu \propto \nu^{-\alpha_\nu}$. This is in agreement with the average value found for MSPs (Kramer et al. 1998; Maron et al. 2000) ($\alpha_\nu = 1.6$ – 1.8), while Bates et al. (2013) found $\alpha_\nu = 1.4$ for slowly rotating pulsars.

In Figure 15 we show the detectability predictions for GBT observations at 850 MHz, 2 GHz, and 5 GHz, respectively. While at 850 MHz the effect of scattering prevents the

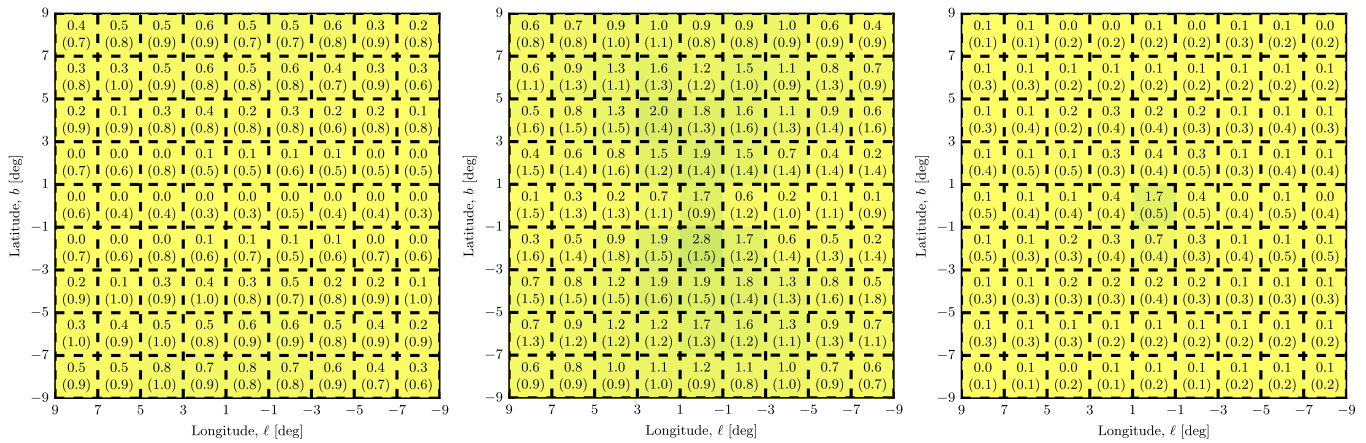


Figure 15. Same as Figure 7, but for a survey performed with theGBT at 850 MHz (left panel), 2 GHz (central panel), or 5 GHz (right panel).

detection of sources in the inner region of the Galaxy and, in particular, along the Galactic plane, 2 GHz turns out to probably be the optimal frequency for large area surveys at mid- and low-latitudes.¹⁸ Indeed, at 2 GHz, on the one hand, the relevance of scattering is reduced with respect to 1.4 GHz (as seen by comparing the number of sources detected in the Galactic plane and in the subregion around the Galactic center) and, on the other hand, the reduction of the signal flux is not as relevant as at 5 GHz. At 5 GHz, indeed, the number of sources that can be detected with the same observation time is much smaller than the number of sources detectable at 2 GHz for all $2^\circ \times 2^\circ$ subregions. The only exception is the region centered on the Galactic center where the effect of scattering is still relevant, in agreement with the latest works considering the detectability of MSPs at the Galactic center (Macquart & Kanekar 2015). However, these central sources are only detectable if they lie in the low-scattering tail of the scattering-time-DM relation. This, and hence the detection prospects in the inner 1 deg, are very uncertain. We note that past radio surveys of the GC region at high frequencies (see for example Johnston et al. 2006; Deneva et al. 2009) were intended to find pulsars at the GC in the very inner degree or less with a very narrow field of view, and thus they were not sensitive to MSPs detection, as explained in Macquart & Kanekar (2015).

As described above, we assume that *all* of the gamma-ray emission from the considered globular clusters comes from MSPs. In the case of e.g., NGC 6440, which contains a young pulsar that is very bright in radio, it could be that the dominant part of the observed gamma-ray emission is actually due to this young pulsar or another source along the line of sight (Abdo et al. 2010). In that case, namely if we neglect NGC 6440 with its very high gamma-ray luminosity in our analysis, our estimate in Equation (2) would systematically *decrease*. This would then *increase* the number of predicted radio-bright MSPs in the bulge in the case at hand by a factor of 1.5 and thus make our predictions more optimistic.

Finally, we comment on another relevant wavelength for MSP studies, namely X-rays. The observation of MSPs in the X-ray band has been pursued by several experiments in the past, and recently by the *Chandra* and *XMM-Newton* observatories. Up to now, 62 MSPs (with period $P < 20$ ms)

have been detected (Prinz & Becker 2015). MSPs are very faint X-ray sources with typical luminosities ranging from $L_X \sim 10^{30} - 10^{31}$ erg s⁻¹. For this reason their detection in the X-ray band is challenging and requires very deep exposures. A large fraction of the MSPs detected in X-rays belongs to globular clusters (Bogdanov et al. 2006). In general, no systematic differences exist between MSPs in globular clusters and those in the field of the Galaxy (Bogdanov et al. 2006). MSPs around the Galactic center are very difficult to probe via soft X-rays (0.5–2 keV) since their faint emission would be mostly absorbed by the intervening material. The hard spectral component could be seen by *NuSTAR*, which in turn suffers from poor angular resolution and makes it difficult to determine whether the source is an MSP (Perez et al. 2015). The need for very deep exposures combined with the typical angular resolution of current X-ray observatories (i.e., 0.5 arcsec for *Chandra* and 6 arcsec for *XMM-Newton*) makes the exploration of a single $2^\circ \times 2^\circ$ sky area (e.g., see Figure 7) very time consuming. The discovery of a bulge population by means of X-ray campaigns seems, therefore, unfavored with respect to present day and next generation radio telescopes.

7. CONCLUSIONS

It has been proposed that the extended excess of GeV photons that was found in *Fermi*-LAT data from the inner Galaxy is caused by the combined emission of a large number of hitherto undetected MSPs in the Galactic bulge. We presented the first comprehensive study of the prospects for detecting radio pulsations from this new MSP population. Based on observations of globular clusters, which we consider as *versions in miniature* of the MSP bulge population, we constructed a radio emission model for the bulge population as a whole. We found a loose correlation between the gamma-ray and radio emission of individual sources in a flux-limited sample of high-latitude *Fermi* MSPs and unassociated sources. We quantitatively showed how existing radio pulsar surveys are not quite sensitive enough to detect a first sample of MSPs from the bulge population. Finally, we discussed in detail how future *deep targeted searches* as well as *large area surveys* can detect the bulge MSPs as a distinct population with high confidence in the upcoming years. Our main findings can be summarized as follows.

¹⁸ We mention however that wide-area surveying at 2 GHz is more challenging, because the beam is even smaller than at 1.4 GHz.

(1) *Fermi*-LAT data from the inner Galaxy suggests that around ~ 3000 radio-bright MSPs ($S_{1.4\text{ GHz}} > 10 \mu\text{Jy}$) are present as a distinct population in the Galactic bulge.

Our estimates are based on an extrapolation of the gamma-ray and radio emission of six globular clusters. The largest uncertainties come from the details of diffuse gamma-ray emissions from the inner 200 pc of the Galactic center, and the actual spatial extent of the MSP bulge population beyond 1.5 kpc.

(2) The expected *surface density* of radio-bright bulge MSPs a few degrees above and below the Galactic center can be determined with good accuracy.

For instance, at Galactic longitudes $\ell \simeq 0^\circ$ and latitudes $|b| \simeq 5^\circ$, we predict a surface density of radio-bright bulge MSPs of $(4.7 \pm 1.5) \text{ deg}^{-2}$. This quoted error takes into account uncertainties related to the radio luminosity function, sampling variance of the relatively small numbers of MSPs in globular clusters, the diffuse gamma-ray emission from the inner Galaxy, and the gamma-ray emission from globular clusters. Closer to the Galactic center the surface density becomes much higher (but so do the challenges of finding millisecond radio pulsations).

(3) We find that frequencies around 1.4 GHz are best for radio pulsation searches for bulge MSPs at mid-latitudes. The effects of scatter-broadening at these frequencies are rather large in the Galactic plane. Detection prospects are hence best at intermediate Galactic latitudes, $2^\circ \lesssim |b| \lesssim 8^\circ$.

Due to broadening from scattering, observations at lower frequencies (850 MHz) yield, in general, a worse result, whereas observations at 5 GHz suffer from the pulsar's intrinsically decreased flux. Optimal frequencies are in the range of 1.4–2.0 GHz. At intermediate latitudes, the most sensitive large area survey in the inner Galaxy is the Parkes HTRU survey at 1.4 GHz. The brightest bulge MSPs with a few hundred μJy just scratch the sensitivity of this survey, which is consistent with current results.

(4) Deep targeted observations of *Fermi* unassociated sources at mid-latitudes with the GBT, and with integration times per pointing of around one hour, can likely lead to the first discoveries of bulge MSPs.

We show that *Fermi* observations of nearby MSPs and bright unassociated sources at high Galactic latitudes suggest a loose but significant correlation between the MSP gamma-ray and radio luminosities. Taking this relation into account, we estimate that there is roughly an 18% probability (with uncertainties of at least a factor of two) that a 1 hr deep observation with GBT at 1.4 GHz could detect a bulge MSP that is seen in gamma-rays. The success of such a targeted campaign will crucially depend on the careful preparation of a list of promising targets.

(5) In the upcoming years, large area surveys using e.g., MeerKAT, and later SKA, can cover a hundred square degrees within a hundred hours of observation time, and they should find dozens to hundreds of bulge MSPs both in the inner few degrees of the Galactic center and up 10° Galactic latitude or more.

Thanks to the much larger field of view and gain, the prospects for detecting a large number of bulge MSPs with upcoming radio telescopes are excellent. The largest limitation of these searches will likely not directly come from the instrumental capabilities but from the enormous computing time required to process all recorded data.

(6) We showed that, for observations a few degrees off the Galactic plane, the detection of $\gtrsim 4$ MSPs with a DM $\sim 300\text{--}400 \text{ pc cm}^{-3}$ at latitudes around $|b| \sim 5^\circ$ could already be enough to detect the bulge component above the thick-disk MSP population with high statistical significance.

The bulge MSP population would increase the number of MSPs that are detectable at 7–10 kpc distances in the inner Galaxy by a large factor with respect to the expectations from only a thick-disk population, and hence, at mid-latitudes, easily identifiable as a distinct population. However, due to the large scatter-broadening, even with SKA, it will remain rather challenging to detect bulge MSPs in the inner 1 deg of the Galactic center (although a few sources might lie along lines-of-sights with reduced scattering). It is hence rather likely that in the foreseeable future the *Fermi* observations of diffuse gamma-rays from the Galactic center will continue to provide the best (though somewhat indirect) constraints on a possible MSP bulge population in the inner ~ 200 pc of the Galactic center.

In summary, if the *Fermi* GeV excess is indeed due to a population of MSPs in the Galactic bulge, the first discovery of this bulge population could be achieved with current technology in the next couple of years. Such a discovery would likely be based on targeted radio searches in *Fermi* unassociated sources or source candidates just below the 3FGL threshold. It is now most pressing to build a list of the most promising targets from *Fermi* gamma-ray data, with reliable probabilistic statements about possible source types.

In the more distant future, on the timescale of at least five years and more, large area surveys with upcoming radio instruments should start to detect many dozens or even hundreds of bulge MSPs. The scientific implications of such detections would be significant. They would allow a systematic study of a potentially very large sample of field MSPs in the bulge, of their gamma-ray and radio emission properties, and of their formation history. They would clarify the origin of the long-debated *Fermi* GeV excess, and allow to disentangle emission from unresolved point sources from the truly diffuse emission from the Galactic bulge, with possible contributions from the *Fermi* bubbles, the activity of the supermassive black hole, or even a signal from dark matter annihilation. Lastly, they would open a completely new window for the systematic study of the formation history of the Galactic bulge and center, and the objects that they contain.

We very warmly acknowledge discussions with Francesco Massaro about multi-wavelength associations of unassociated *Fermi* sources. We furthermore acknowledge useful discussions with Jonathan E. Grindlay, Tim Linden, Scott Ransom, Marco Regis, Pasquale D. Serpico, and Meng Su in different stages of the project. J.W.T.H. acknowledges funding from an NWO Vidi fellowship and from the European Research Council under the European Union's Seventh Framework Programme (FP/2007-2013)/ERC Starting Grant agreement nr. 337062 ("DRAGNET"). F.C. and C.W. acknowledge funding from an NWO Vidi fellowship.

APPENDIX A MULTI-WAVELENGTH STUDY OF MSP CANDIDATES IN FERMI DATA

Based on a spectral matching analysis, Bartels et al. (2015) identified 13 sources in the 3FGL catalog (Acero et al. 2015) as

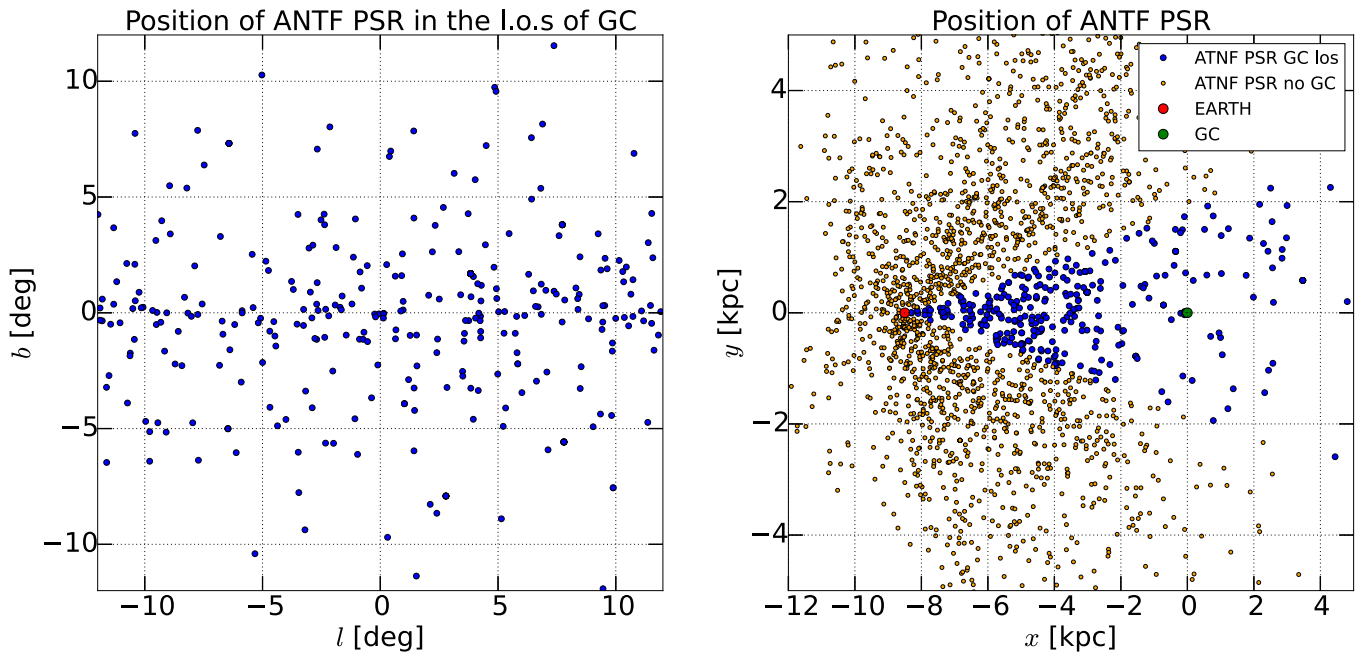


Figure 16. Positions of the ATNF catalog pulsars in the $|l| < 12^\circ$ and $2^\circ < |b| < 12^\circ$ region. Left panel: catalog sources are displayed as blue points in the longitude-latitude plane. Each position in the plane corresponds to an observation of a line of sight. Right panel: all catalog sources are displayed as gold points. They are projected onto the Galactic plane, knowing their distance from the Earth (identified by a red point), and located by their Galactic coordinates (the Galactic center is identified by a green point). The sources displayed in the left panel are depicted as blue points.

candidates for MSPs in the inner Galaxy ($|l| < 12^\circ$ and $2^\circ < |b| < 12^\circ$). The criterion was that the spectrum of the sources is roughly compatible with the spectrum of the stacked MSPs from Cholis et al. (2014), and that they show no significant variability. We stress that the *raison d’être* for this source list is *not* to find the best MSP candidates for radio follow-up searches (this requires a more detailed study that will be presented elsewhere), but simply to remove a bias in the wavelet analysis from Bartels et al. (2015) by unmasking some of the 3FGL sources that might be part of the bulge population. However, we will analyze here the properties of these 13 sources, as well as some of the other wavelet peaks found in this analysis to *first* confirm that an MSP interpretation of the 13 sources as well as the significant wavelet peaks is compatible with multi-wavelength data, and *second* to demonstrate the potential and limitations that such multi-wavelength studies of MSP candidates in the inner Galaxy entail.

A.1. Cross-correlation of Gamma-ray MSP Candidates and Known Radio Pulsars

In the recent analysis of the inner Galaxy by Bartels et al. (2015), which adopted a wavelet decomposition of the gamma-ray sky to search for sub-threshold point sources, a significant clustering of photons compatible with the unresolved gamma-ray emission from a bulge population of MSPs as suggested by *Fermi*-LAT data has been observed. The region of interest (ROI) of the analysis is defined by $|l| < 12^\circ$ and $2^\circ < |b| < 12^\circ$. The signal-to-noise ratio of the wavelet transforms at position Ω , $\mathcal{S}(\Omega)$ (Equation (2) in Bartels et al. 2015), and is a rough measure of the local significance for having a source at position Ω in units of standard deviations. The peaks in $\mathcal{S}(\Omega)$ considered in the wavelet search have significances in the range $1 \leq \mathcal{S} \leq 10$. In particular, the peaks

with $\mathcal{S} > 3$ may be considered as promising targets for radio follow-up searches for radio MSPs.

If the more significant gamma-ray wavelet peaks from Bartels et al. (2015) are indeed identified with a bulge MSP population, they should not be correlated with foreground sources. We explore this possibility by studying the correlation between the radio pulsars in the ATNF catalog (Manchester et al. 2005) and the wavelet peaks with $\mathcal{S} > 2$ and $\mathcal{S} > 3$. Within the main ROI, the pulsar ATNF catalog contains 331 pulsars with a measurement of the distance. However, we will study potential correlations not only in the inner Galaxy ROI, but also in the control regions along the Galactic disk from Bartels et al. (2015), centered in $l = \pm k \cdot 20^\circ$ and $b = 0^\circ$, with $k = 1, 2, 3, 4$ and with the same extension of the Galactic center region.

We consider here the same wavelet peaks as in Bartels et al. (2015). That means from the total number of identified wavelet peaks we subtract: (i) all sources that spatially coincide with associated sources from the 3FGL catalog (Acero et al. 2015); (ii) all unassociated sources with a non-pulsar spectrum, according to the same criterion as described in (Bartels et al. 2015).

We derive for each ROI (main and control) the number of positional correlations between the gamma-ray wavelet peaks and the ATNF sources. For the threshold distance for the correlation we tested two values, 0.1° and 0.2° . The first angle cut is equal to the largest value of the 95% containment angle (Conf95_SemiMajor in the 3FGL catalog), which is an indicator of the positional error of point sources. The second value, 0.2° , has been considered because most of the gamma-ray peaks are just below the detection threshold and so the 95% containment angle parameter for them is effectively larger. However, we found similar results and will only use 0.1° in the following.

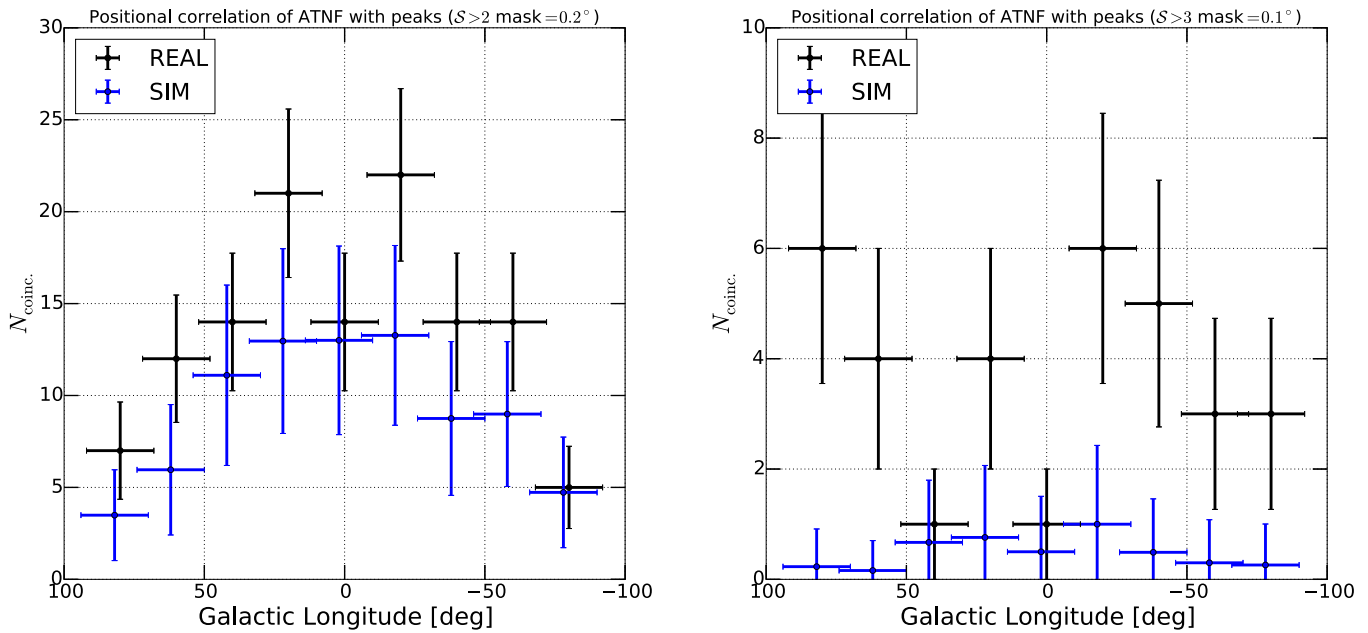


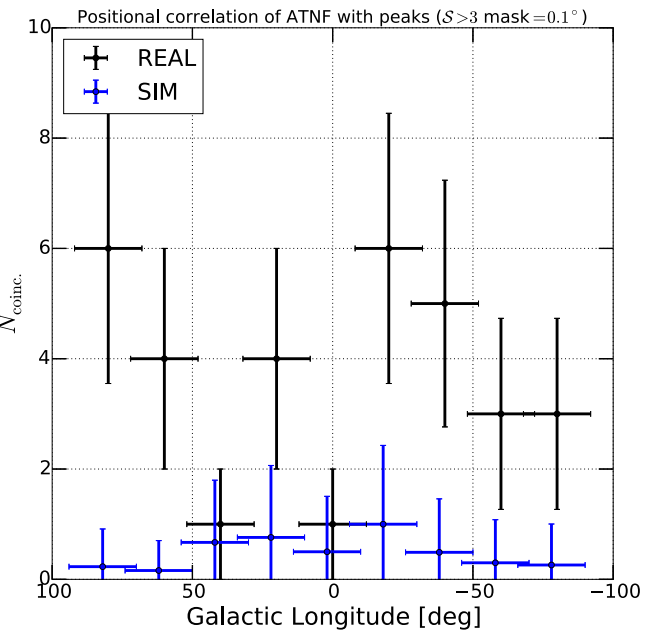
Figure 17. Number of positional correlations between the gamma-ray wavelet peaks and the sources in the ATNF catalog, as a function of the Galactic longitude, for latitudes $2^\circ < |b| < 12^\circ$. The left (right) panels correspond to the peaks with significance $\mathcal{S} > 2$ ($\mathcal{S} > 3$). The black points represent the correlations found from the real gamma-ray wavelet peak catalog as discussed in the text, while the blue ones are derived from a reshuffling in latitude bins. The analysis is performed for threshold angles 0.2° (left) and 0.1° (right).

In Figure 17 we plot the number of positional correlations as a function of the longitudinal ROI position. For the gamma-ray wavelet peaks we have chosen the significance $\mathcal{S} > 2$ and $\mathcal{S} > 3$. The results are plotted as black error bars, and actually fluctuate strongly from ROI to ROI. The error bars are defined as the Poissonian error on the number of correlations.

We have also estimated the number of positional correlations that one would expect from a random positioning of the wavelet peaks in each of the analyzed sky regions. In order to derive this test population we used “scrambled data” and changed the longitude and latitude of each wavelet peak randomly in the interval $[l - 2^\circ, l + 2^\circ]$ and $[b - 1^\circ, b + 1^\circ]$. In this way, we largely preserve the observed spatial distribution of the peaks, which is concentrated along the Galactic disk.

The cross-correlation that we find between the ATNF sources and our scrambled test wavelet sample are shown by the blue error bars in Figure 17. Interestingly, for both $\mathcal{S} > 2$ and even more so for $\mathcal{S} > 3$, we find in most ROIs an excess of correlations above what is randomly expected, with the exception of the Galactic center and a region around $\ell \approx 40^\circ$. This strongly suggests that some of the wavelet peaks are actually caused by the emission of pulsars that are already part of the ATNF, but not the 3FGL. We note that the number of *potential* correlations in each ROI is much larger than what we find.

The variations in the correlation between wavelet peaks and ATNF sources that we find in most of the control regions away from the Galactic center suggest that, along the Galactic plane, a number of radio pulsars remained below the *Fermi* detection threshold up to now, but showed up as wavelet peaks in our analysis. This effect depends on the general pulsar density in a certain direction, and happens to be small toward the inner Galaxy.



APPENDIX B AN ANALYSIS OF 13 GAMMA-RAY UNASSOCIATED SOURCES IN THE INNER GALAXY

We will, in the following study, explain in some detail the properties of the 13 unassociated 3FGL sources that were identified in Bartels et al. (2015) as MSP candidates (see their Table 1). We stress again that this does not imply that these sources would be the best targets for radio follow-up searches. Instead, the discussion below will show what is generally possible with spectral and multi-wavelength analyses.

B.1. Gamma-Ray Spectral Analysis

We study here the gamma-ray SED of these MSP candidates. To this end, we perform a fit to their gamma-ray spectra as given in the 3FGL catalog (Acero et al. 2015), in the energy range 0.1–100 GeV. We adopt a power-law with an exponential cutoff, which is the typical gamma-ray SED of pulsars,

$$\frac{dN}{dE} = K_0 \left(\frac{E}{E_0} \right)^{-\Gamma} \exp\left(-\frac{E}{E_{\text{cut}}} \right), \quad (7)$$

where K_0 is the normalization of the spectrum, E_0 is the pivot energy, Γ is the photon index, and E_{cut} is the energy cutoff. In order to check if those sources could be spectrally associated with AGNs (although, as discussed in Bartels et al. (2015), this is a priori not very likely given the low average number density of AGNs in the Galactic disk), we consider two different cases for the range of variability of the photon index and the energy cut off. We stress that for pulsars and AGNs, the model parameters are usually strongly correlated, which we neglect here for simplicity, however.

Table 5

Results for the Fits to the Gamma-Ray Spectra of the 13 Unassociated 3FGL Sources from Bartels et al. (2015), Using 3FGL Catalog Spectral Data and Two Different Assumptions for the SED Parameters (See Text for Details)

3FGL Source	Γ^{PSR}	$E_{\text{cut}}^{\text{PSR}}$ (GeV)	$\tilde{\chi}_{\text{PSR}}^2$	Γ^{AGN}	$E_{\text{cut}}^{\text{AGN}}$ (GeV)	$\tilde{\chi}_{\text{AGN}}^2$
J1649.6-3007	>1.90	>5.5	0.88	2.15 ± 0.25	25 ± 5	0.15
J1703.6-2850	1.49 ± 0.36	>5.5	1.15	1.94 ± 0.24	25 ± 4	0.32
J1740.5-2642	1.54 ± 0.44	3.1 ± 1.6	0.08	1.94 ± 0.14	<7	0.66
J1740.8-1933	>1.9	>5.5	2.4	2.13 ± 0.20	>200	0.22
J1744.8-1557	>1.9	4.7 ± 3.6	0.17	2.17 ± 0.58	10 ± 3	0.08
J1758.8-4108	<0.7	1.8 ± 0.3	1.91	1.85 ± 0.35	21 ± 6	2.28
J1759.2-3848	1.52 ± 0.22	>5.5	0.18	1.96 ± 0.18	>270	0.24
J1808.3-3357	1.37 ± 0.32	2.5 ± 1.0	0.08	1.84 ± 0.11	<7	1.28
J1808.4-3519	>1.90	>5.5	0.32	2.03 ± 0.51	8.1 ± 3.0	0.27
J1808.4-3703	1.46 ± 0.15	2.7 ± 0.6	0.022	1.93 ± 0.19	<7	0.64
J1820.4-3217	1.60 ± 0.35	2.7 ± 1.0	0.41	2.05 ± 0.13	<7	0.21
J1830.8-3136	<0.70	1.8 ± 0.3	0.75	<1.75	9.4 ± 3.0	1.80
J1837.3-2403	1.73 ± 0.24	>5.5	0.48	1.97 ± 0.57	13 ± 5	0.50

1. Pulsar-like. The average value for Γ and E_{cut} for pulsars in the *Fermi*-LAT catalogs (see e.g., Abdo et al. 2013) are $\Gamma = 1.30 \pm 0.30$ and $\log_{10}(E_{\text{cut}}/\text{MeV}) = (3.38 \pm 0.18)$, respectively. We therefore restrict the photon index in range $\Gamma \in [0.70, 1.90]$ and the energy cutoff $E_{\text{cut}} \in [1.5, 5.50]$ GeV, according to the 95% CL limits of their observed distributions. Note that this entails the spectra of both young and recycled pulsars.
2. Flat Spectrum Radio Quasar (FSRQ) like. We have performed a fit to the FSRQ sources in the 3FGL catalog Acero et al. (2015) with a detection significance large than six, with the SED assumed to be a power-law with an exponential cutoff (Equation (7)). The best-fit parameters are $\Gamma = 2.25 \pm 0.25$ and $E_{\text{cut}} = 30_{-16}^{+120}$ GeV, and the fit has a reduced chi-square $\tilde{\chi}^2 = 0.72$. We therefore restrict the photon index to the 95% CL range $\Gamma \in [1.75, 2.75]$ and $E_{\text{cut}} \in [8.0, 270]$ GeV.

The fit results are summarized in Table 5 in terms of the photon index, Γ , and the exponential cutoff, E_{cut} , best-fit values for each of the 13 sources, both for the pulsar and the AGN priors on the free parameters. We also indicate the goodness-of-fit by the $\tilde{\chi}^2 = \chi^2/\text{dof}$, where the degrees of freedom are $\text{dof} = 5-3$. For most of the sources, we find rather small values for $\tilde{\chi}^2$, which indicates that the fluxes are over-fitted, likely related to the low number of energy bins or the large statistical error bars of the fluxes, which precludes any statements about what spectra are preferred. In a few cases, the $\tilde{\chi}^2$ is significantly above 1.0; values above around 2.3 would indicate a 90% CL tension between model and measured spectrum. This is only the case for J1740.8-1933, which is mildly inconsistent with a pulsar spectrum, and J1758.8-4108, which is mildly inconsistent with an AGN spectrum. We conclude that spectral information alone, in the way we use it here, is not enough to make strong statements about the nature of the source. However, if we simply interpret the results as indicative for a possible source type, six sources might be more pulsar-like, and six sources more AGN-like. A more detailed study, taking into account parameter correlations and a larger range of spectral bins, is warranted but beyond the scope of the current work.

B.2. Multi-wavelength Properties from X-Ray and Radio

Recent multi-frequency analyses (see e.g., Massaro et al. 2013) supported by optical follow-up spectroscopic campaigns (see e.g., Massaro et al. 2014) on different samples of unassociated gamma-ray sources have been extremely successful to find new blazar-like counterparts as well as to exclude their presence (see e.g., Massaro et al. 2015, and references therein)

For all the 13 unidentified gamma-ray sources in Bartels et al. (2015) we investigated several catalogs and surveys, spanning the whole electromagnetic spectrum, and searched for potential low-energy counterparts that could either help to confirm or provide information on the pulsar-like nature/behavior of these sources. We reduced the X-ray observations available in the *SWIFT* archive and obtained with the follow-up program on the unassociated *Fermi*-LAT objects.

In particular, since each associated gamma-ray blazar has a radio counterpart, we first investigated the NRAO VLA Sky Survey that cover the footprint of these 13 objects (Condon et al. 1998) to exclude or confirm the possible presence of blazar-like potential counterparts within the *Fermi* positional uncertainty. This has been also motivated by the success of the follow-up radio observations performed since the launch of *Fermi* (e.g., Schinzel et al. 2015). We also searched in low frequency radio observations (i.e., below ~ 1 GHz) for blazar-like source.

3FGL J1703.6-2850—This *Fermi*-LAT source has a single unidentified radio object (NVSS J170341-285343) lying within the positional uncertainty region at a 95% level of confidence. According to the NVSS radio image, NVSS J170341-285343 has compact radio structure also showing a jet-like component that could resemble of a blazar-like nature. This radio source has also an optical counterpart in the USNO catalog. In the X-ray images obtained by *SWIFT* there are no objects detected with a signal-to-noise ratio greater than three.

3FGL J1740.5-2642—There are two radio sources lying within the positional uncertainty region of this unassociated *Fermi*-LAT object. However, the first source, NVSS J174012-264422, is a planetary nebula (aka ESO 520 PN-015) and thus is unlikely to be the low-energy counterpart of 3FGL J1740.5-2642. The other one, NVSS J174039-264541, is a simple,

bright (flux density at 1.4 GHz of 14.7 mJy), radio source with a compact structure having also an optical correspondence in the USNO catalog.

3FGL J1740.8-1933—For *3FGL J1740.8-1933*, as in the previous case, there are two compact radio sources lying within the positional uncertainty region at a 95% level of confidence: NVSS J174051-193011 and NVSS J174105-193006. None of them has an optical counterpart but the latter is also detected in the *WISE* all-sky survey, even if its IR colors are not consistent with those of the *Fermi*-LAT detected blazars. No sources are detected in the X-rays as paper in the *SWIFT* observations.

3FGL J1744.8-1557—There are five radio sources in the NVSS catalog that lie within the positional uncertainty region of *3FGL J1744.8-1557*. Two of them are also detected in the *WISE* all-sky survey, NVSS J174509-155000 and NVSS J174443-160531, but they do not have IR colors similar to the *Fermi*-LAT blazars. In addition, NVSS J174437-160253 shows an extended structure while all the others appear to be compact in the NVSS radio images. None of them is detected in the X-rays.

3FGL J1759.2-3848—Three radio sources reported in the NVSS catalog, all compact, are present in the line of sight of this source. The most interesting one is probably NVSS J175926-384753 that lies only 136 arcsec from the gamma-ray position of *3FGL J1759.2-3848*, and has both an IR and an optical counterpart. None of them is detected in the X-rays. There is only one source in the *SWIFT*-XRT image but it corresponds to a bright star in the field of view clearly detected in the optical and ultraviolet images of the UVOT instrument on board *SWIFT*.

3FGL J1808.4-3703—This source is remarkably interesting because within its positional uncertainty region at a 95% level of confidence there is a known X-ray transient: SAX J1808.4-3658. This is an accreting MSPS, in which the neutron star is orbiting around a brown dwarf companion. A recent and detailed X-ray analysis of all the archival *SWIFT*-XRT observations is presented in Campana et al. (2008).

3FGL J1820.4-3217—This is the unique source for our sample for which the gamma-ray spectral properties have been investigated with a statistical approach. The results provided by a classification tree method support the idea that the gamma-ray behavior of this source resembles that of an active galaxy rather than a pulsar. There is a radio source (i.e., NVSS J182045-321621) lying within its positional uncertainty region that presents a faint extended structure and has an infrared and an optical potential counterpart at ~ 12 arcsec distance from the radio core position. This NVSS object is not detected in the X-rays.

3FGL J1830.8-3136—Four radio sources are detected within the region of interest for *3FGL J1830.8-3136*, in particular, NVSS J183027-313738 shows a compact structure, but the other two radio objects, NVSS J183038-313506 and NVSS J183033-313608, appear to be knots of a jet-like extended structures of $0^{\circ}.06$ length. NVSS J183027-313738 is also detected in the optical but does not have an IR counterpart in the *WISE* all-sky survey.

3FGL J1837.3-2403—Approximately $0^{\circ}.2$ from the position of the *Fermi*-LAT source, and less than $0^{\circ}.1$ distance from the border of its elliptical positional uncertainty region having a major axis of $0^{\circ}.2$, there is a well known globular cluster: M22. Unfortunately the *SWIFT* XRT image is centered on the globular cluster and thus it is completely covering the *Fermi*-

LAT region of interest, so it is not possible to know if there are X-ray sources detected that could be potential counterparts of the gamma-ray object.

3FGL J1649.6-3007, *3FGL J1758.8-4108*, and *3FGL J1808.4-3519*—No X-ray sources are detected within the positional uncertainty region of this *Fermi*-LAT source in the *SWIFT* image. In addition, there are no radio sources within the same region of interest and no *WISE* sources with IR colors similar to gamma-ray blazars.

3FGL J1808.3-3357—There are 3 X-ray sources and among them one is NOVASGR20093.

REFERENCES

- Abazajian, K. N. 2011, *JCAP*, **1103**, 010
- Abazajian, K. N., Canac, N., Horiuchi, S., & Kaplinghat, M. 2014, *PhRv*, **D90**, 023526
- Abazajian, K. N., & Kaplinghat, M. 2012, *PhRv*, **D86**, 083511
- Abdo, A., Ackerman, M., Ajello, M., et al. 2010, *A&A*, **524**, A75
- Abdo, A., Ajello, M., Allafort, A., et al. 2013, *ApJS*, **208**, 17
- Acerro, F., Ackerman, M., Ajello, M., et al. 2015, *ApJS*, **218**, 23
- Aharonian, F., Akhperjanian, A. G., Aye, K.-M., et al. 2004, *A&A*, **425**, L13
- Aharonian, F. A., Atayan, A. M., & Kifune, T. 1997, *MNRAS*, **291**, 162
- Ajello, M., Albert, A., Atwood, W. B., et al. 2016, *ApJ*, **819**, 44
- Alpar, M. D. R., Cheng, A. F., Ruderman, M. A., & Shaham, J. 1982, *Natur*, **300**, 728
- Arca-Sedda, M., & Capuzzo-Dolcetta, R. 2014, *MNRAS*, **444**, 3738
- Bagchi, M., Lorimer, D. R., & Chennamangalam, J. 2011, *MNRAS*, **418**, 477
- Barr, E. D., Guillemot, L., Champion, D. J., et al. 2013, *MNRAS*, **429**, 1633
- Bartels, R., Krishnamurthy, S., & Weniger, C. 2016, *PhRvL*, **116**, 051102
- Bates, S. D., Lorimer, D. R., & Verbiest, J. P. W. 2013, *MNRAS*, **431**, 1352
- Bednarek, W., & Sobczak, T. 2013, *MNRAS*, **435**, L14
- Bhat, N. D. R., Cordes, J. M., Camilo, F., Nice, D. J., & Lorimer, D. R. 2004, *ApJ*, **605**, 759
- Bhattacharya, D., & van den Heuvel, E. P. J. 1991, *PhR*, **203**, 1
- Bogdanov, S., Grindlay, J. E., Heinke, C. O., et al. 2006, *ApJ*, **646**, 1104
- Brandt, T. D., & Kocsis, B. 2015, *ApJ*, **812**, 15
- Calore, F., Cholis, I., McCabe, C., & Weniger, C. 2015a, *PhRv*, **D91**, 063003
- Calore, F., Cholis, I., & Weniger, C. 2015b, *JCAP*, **1503**, 038
- Calore, F., Di Mauro, M., Donato, F., & Donato, F. 2014, *ApJ*, **796**, 14
- Camilo, F., Lorimer, D. R., Freire, P., Lyne, A. G., & Manchester, R. N. 2000, *AJ*, **535**, 975
- Camilo, F., Kerr, M., Ray, P. S., et al. 2015, *ApJ*, **810**, 85
- Campana, S., Stella, L., & Kennea, J. A. 2008, *ApJL*, **684**, L99
- Carlson, E., Linden, T., & Profumo, S. 2016, arXiv:1603.06584
- Carlson, E., & Profumo, S. 2014, *PhRv*, **D90**, 023015
- Cheng, K. S., Taam, R. E., & Wang, W. 2004, *ApJ*, **617**, 480
- Chevalier, R. A. 2000, *ApJ*, **539**, L45
- Cholis, I., Evoli, C., Calore, F., et al. 2015, *JCAP*, **12**, 005
- Cholis, I., Hooper, D., & Linden, T. 2014, arXiv:1407.5583
- Condon, J. J., Cotton, W. D., Greisen, E. W., et al. 1998, *AJ*, **115**, 1693
- Cordes, J. M., & Lazio, T. J. W. 2002, arXiv:astro-ph/0207156
- Cowan, G., Cranmer, K., Gross, E., & Vitells, O. 2011, *EPJC*, **71**, 1554
- Daylan, T., Finkbeiner, D. P., Hooper, D., et al. 2016, *ApJL*, **702**, L177
- Deneva, J. S., Cordes, J. M., & Lazio, T. J. W. 2009, *ApJ*, **702**, L177
- Dewey, R., Stokes, G., Segelstein, D., Taylor, J., & Weisberg, J. 1984, Birth and Evolution of Neutron Stars: Issues Raised by Millisecond Pulsars, ed. S. P. Reynolds & D. R. Stinebring, 234
- Faucher-Giguère, C.-A., & Kaspi, V. M. 2006, *ApJ*, **643**, 332
- Faucher-Giguère, C.-A., & Loeb, A. 2010, *JCAP*, **1**, 5
- Gaggero, D., Urbano, A., Valli, M., & Ullio, P. 2015, *PhRv*, **D91**, 083012
- Gillessen, S., Eisenhauer, F., Trippe, S., et al. 2009, *ApJ*, **692**, 1075
- Gnedin, O. Y., Ostriker, J. P., & Tremaine, S. 2014, *ApJ*, **785**, 71
- Gordon, C., & Macias, O. 2013, *PhRv*, **D88**, 083521
- Grenier, I. A., & Harding, A. K. 2015, *Comptes Rendus Physique*, **16**, 641
- Haslam, C. G. T., Salter, C. J., Stoffel, H., & Wilson, W. E. 1982, *A&AS*, **47**, 1
- Hessels, J. W. T., Ransom, S. M., Stairs, I. H., Kaspi, V. M., & Freire, P. C. C. 2007, *ApJ*, **670**, 363
- Hooper, D., & Goodenough, L. 2011, *PhL*, **697**, 412
- Hooper, D., & Goodenough, L. 2014, *PhL*, **B697**, 412
- Hooper, D., & Linden, T. 2011, *PhRv*, **D84**, 123005
- Johnston, S., Kramer, M., Lorimer, D. R., et al. 2006, *MNRAS*, **373**, L6
- Kalpatharakos, C., Harding, A. K., & Kazanas, D. 2014, *ApJ*, **793**, 97
- Keith, M. J., Jameson, A., van Straten, W., et al. 2010, *MNRAS*, **409**, 619

- Konar, S. 2010, *MNRAS*, **409**, 259
- Kramer, M., Xilouris, K. M., Lorimer, D. R., et al. 1998, *ApJ*, **501**, 270
- Lawson, K. D., Mayer, C. J., Osborne, J. L., & Parkinson, M. L. 1987, *MNRAS*, **225**, 307
- Lee, S. K., Lisanti, M., Safdi, B. R., Slatyer, T. R., & Xue, W. 2015, *PhRvL*, **116**, 051103
- Levin, L., Bailes, M., Barsdell, B. R., et al. 2013, *MNRAS*, **434**, 1387
- Lorimer, D. R., et al. 2015, *MNRAS*, **450**, 2185
- Macias, O., & Gordon, C. 2014, *PhRv*, **D89**, 063515
- Macquart, J.-P., & Kanekar, N. 2015, *ApJ*, **805**, 172
- Manchester, R. N., Hobbs, G. B., Teoh, A., & Hobbs, M. 2005, *AJ*, **129**, 1993
- Maron, O., Kijak, J., Kramer, M., & Wielebinski, R. 2000, *A&AS*, **147**, 195
- Massaro, F., D'Abrusco, R., Paggi, A., et al. 2013, *ApJS*, **206**, 13
- Massaro, F., Masetti, N., D'Abrusco, R., Paggi, A., & Funk, S. 2014, *AJ*, **148**, 66
- Massaro, F., D'Abrusco, F., Landoni, M., et al. 2015, *ApJS*, **217**, 2
- Mayer-Hasselwander, H. A., Bertsch, D. L., Dingus, B. L., et al. 1998, *A&A*, **335**, 161
- McCann, A. 2015, *ApJ*, **804**, 86
- Muno, M. P., Baganoff, F. K., Bautz, M. W., et al. 2003, *ApJ*, **589**, 225
- Ng, C., Bailes, M., Bates, S. D., et al. 2014, *MNRAS*, **439**, 1865
- O'Leary, R. M., Kistler, M. D., Kerr, M., & Dexter, J. 2015, arXiv:1504.02477
- Pallanca, C., Mignani, R. P., Dalessandro, E., et al. 2012, *ApJ*, **755**, 180
- Perez, K., Hailey, C. J., Bauer, F. E., et al. 2015, *Natur*, **520**, 646
- Petrovic, J., Serpico, P. D., & Zaharijas, G. 2014a, *JCAP*, **1410**, 052
- Petrovic, J., Serpico, P. D., & Zaharijas, G. 2014b, *JCAP*, **2015**, 023
- Prinz, T., & Becker, W. 2015, arXiv:1511.07713
- Ransom, S. M. 2001, PhD thesis, Harvard Univ.
- Ray, P., Abdo, A., Parent, D., et al. 2012, arXiv:1205.3089
- Ray, P. S., et al. 2013, *ApJL*, **763**, L13
- Schinzell, F. K., Petrov, L., Taylor, G. B., et al. 2015, *ApJS*, **217**, 4
- Stovall, K., Lorimer, D., & Lynch, R. S. 2013, *CQGra*, **30**, 224003
- Stovall, K., et al. 2014, *ApJ*, **791**, 67
- Strong, A. W. 2007, *Ap&SS*, **309**, 35
- Tremaine, S. D., Ostriker, J. P., & Spitzer, L., Jr. 1975, *ApJ*, **196**, 407
- Venter, C., Johnson, T., Harding, A., & Grove, J. 2014, in Proc. SAIP2013, the 58th Annual Conf. South African Institute of Physics, ed. R. Botha & T. Jili
- Verbunt, F., & Hut, P. 1987, in IAU Symp. 125, The Origin and Evolution of Neutron Stars, ed. D. J. Helfand & J.-H. Huang, 187
- Vitale, V., & Morselli, A. 2009, arXiv:0912.3828
- Wang, W. 2006, *ChJAA*, **6**, 268
- Yuan, Q., & Ioka, K. 2015, *ApJ*, **802**, 124
- Yuan, Q., & Zhang, B. 2014, *JHEAp*, **3-4**, 1
- Zhang, L., & Cheng, K. S. 2003, *A&A*, **398**, 639
- Zhou, B., Liang, Y.-F., Huang, X., et al. 2014, *PhRvD*, **91**, 123010
- Zhou, J. N., Zhang, P. F., Huang, X. Y., et al. 2015, *MNRAS*, **448**, 3215